Design and Manufacture of an Ultra-High Field Ex Vivo Coil Assembly

by

Loren Daniel Bridgers

B.S. Mechanical Engineering
University of New Mexico, 2010

Submitted to the Department of Mechanical Engineering
in Partial Fulfillment of the Requirements for the Degree of

Master of Science in Mechanical Engineering

at the

MASSACHUSETTS INSTITUTE OF TECHNOLOGY

June 2012

Author .....
Department of Mechanical Engineering
May 18, 2012

Certified by .....
Alexander Slocum
Pappalardo Professor of Mechanical Engineering
Thesis Supervisor

Accepted by.....
Professor David E. Hardt
Professor of Mechanical Engineering
Chairman, ME Committee for Graduate Students

Design and Manufacture of an Ultra-High Field Ex Vivo Coil Assembly

by

Loren Daniel Bridgers

Submitted to the Department of Mechanical Engineering on May 18, 2012
in Partial Fulfillment of the Requirements for the Degree of
Master of Science in Mechanical Engineering

Abstract

Magnetic Resonance based architectonic segmentation aims to detect variations in brain architecture that may provide incredible insight into diseases such as epilepsy, schizophrenia, dyslexia, and autism. Data from ex vivo scans is necessary for the development of automatic methods to detect these critical variations in vivo (1) (2). The optimization of ex vivo imaging requires the design and construction of special purpose instrumentation. This thesis presents the mechanical design and construction of a 32 channel ex vivo coil assembly for use in a 7 tesla MRI. The unit will be used for research at the Athinoula A. Martinos Center for Biomedical Imaging in Charlestown, Massachusetts. Also presented is the development and implementation of two unique low-cost tools to enhance the medical instrument prototyping process: a desktop vacuum casting system, and an automatic tool-path generation program for machining directly from STL files. Finally, an improved method and apparatus for degassing the tissue samples is developed and implemented leading to improvements in MRI image quality.

Contents

1. Ex-vivo background

1.1. Ex Vivo Motivation

The aim of MR-based Architectonic Segmentation is to develop MR based tools to analyze the laminar architecture of the cerebral cortex. The cerebral cortex is the folded sheet of neural tissue that forms the outer most surface of the cerebrum. Being able to detect variations or changes in its laminar architecture may provide incredible insight into diseases such as epilepsy, schizophrenia, dyslexia, and autism. The ultimate goal is to be able to automatically define laminar boundaries using high-resolution MRI in hundreds or thousands of samples.

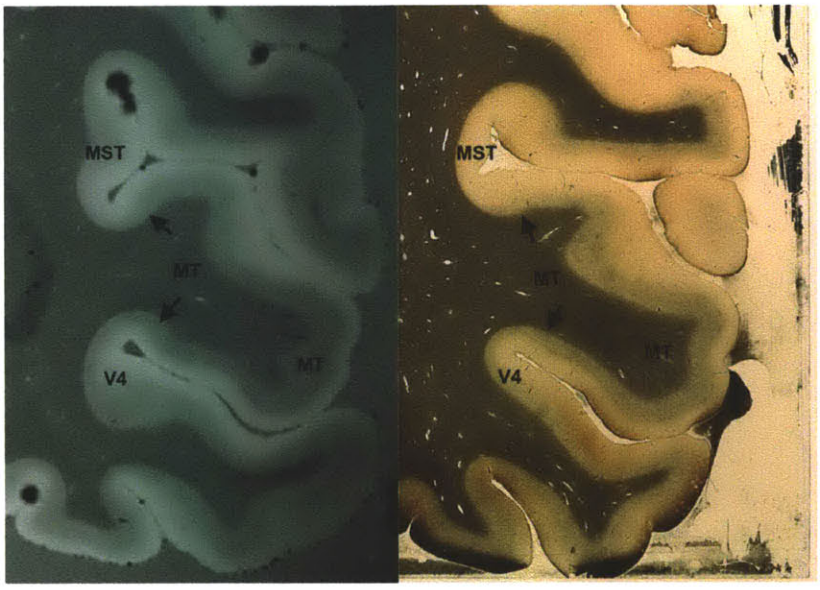

Figure 1

High resolution ex vivo MRI (150um) (left) and corresponding Gallyas myelin stained slice (right). (23)

To achieve this goal, information from ex vivo samples will be used to infer architecture in *in vivo* samples. The immediate goal is to optimize ex vivo imaging to obtain undistorted 100um isotropic images over an entire hemisphere with uniform contrast. Figure 1 shows a high resolution ex vivo MRI used to identify anatomical regions of the cortex compared to a traditional stained slice on the right. Using MRI to define laminar boundaries is very advantageous compared to the traditional, extremely tedious process of manually defining laminar boundaries by cutting and staining which leads to distortion. Figure 1 shows and MRI generated "slice" next to a traditional sample which is manually sliced, stained, and labeled. The optimization of ex vivo imaging requires the design and construction of a special purpose sample holder and ex vivo coil arrays to match. In addition, a process for removing trapped air in

the samples is required. The apparatus used to hold ex vivo samples during imaging is critical to resolution. Spacing between the sensing coils and sample, motion of the sample, and air bubbles in ultra-high field strengths all contribute to reducing the signal to noise ratio.

The 32channel 7T design presented here will be the first 32 channel ex-vivo coil for use at 7T. It will be used at the Athinoula A. Martinos Center for Biomedical Imaging (3).

1.2. MRI Fundamentals

Most Magnetic Resonance Imaging (MRI) acts on the Hydrogen nuclei and its single proton. The basic idea is to disturb the precession of these nuclei then differentiate mater by how long it takes the precessions to relax back to their original motion. The key to MRI is using magnetic gradients to alter precession phase and frequency as a function of position. The spinning nucleus has an intrinsic angular momentum (a property of fundamental particles) and magnetic moment vector $\bar{m}$ due to the electron spin around the nucleus. Just like a top under the influence of gravity, the moment vector of the nucleus will precess around the direction of an external magnetic field. There are three main magnetic fields used in MRI, the first of these is the B_0 field. B_0 is a very strong (in clinical machines 1.5 Tesla - 7 Tesla) static magnetic field which aligns most (those with low enough thermal energy) of the nuclei in the B_0 direction Z down the main magnet bore of the MRI.

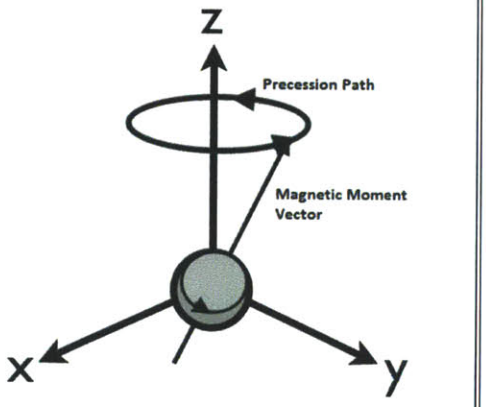

Figure 2 (14)

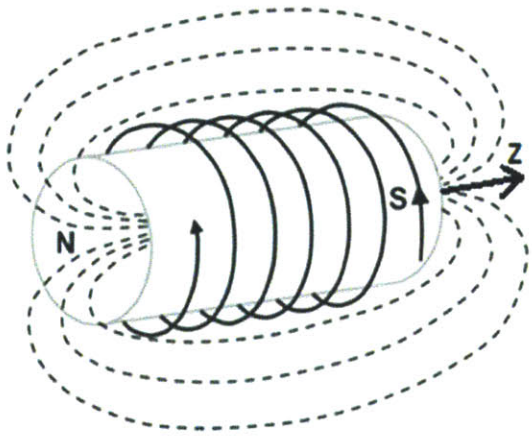

Figure 3 (14)

The external moment applied to the nucleus as a result of $\bar{m}$ and B_0 is $\bar{C} = \bar{m} \times \overline{B_0}$, we also know from dynamics that the sum of external moments equals the time rate of change of the angular momentum vector. $\bar{C} = \bar{m} \times \overline{B_0} = \frac{dI}{dt}$ this leaves us with a differential equation with the solution $I = De^{-i\omega_0 t}$ which oscillates with the frequency $\omega_0 = -\gamma_p^r B_0$ where γ_p^r is a nucleus dependent constant. ω_0 is known as the

Larmor frequency and is the frequency at which the nucleus magnetic moment vector $\bar{m}$ will precess about B_0.

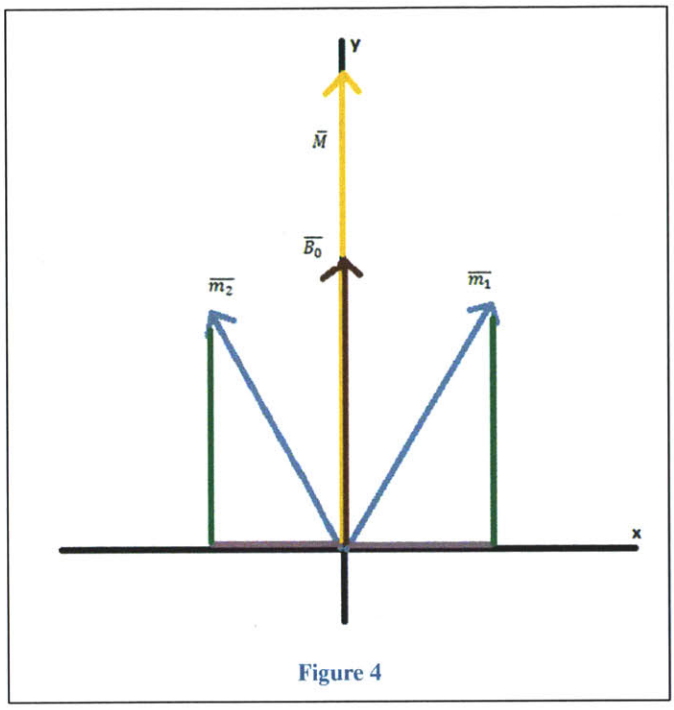

Figure 4

The net magnetization vector $\bar{M}$ is the vector sum of all the individual magnetization vectors $\bar{m}$. It is very important to note that under the presence of the static magnetic field B_0, $\bar{M}$ does not precess. This is because individual nuclei are precessing at random phases, and the x component of their magnetization moment is canceled by other nuclei's magnetization moments that are out of phase. Figure 4 shows how the magnetization vectors of two nuclei precessing 180° out of phase (both precess about B_0) would cancel in the x direction and the net magnetization vector is the sum of the y components.

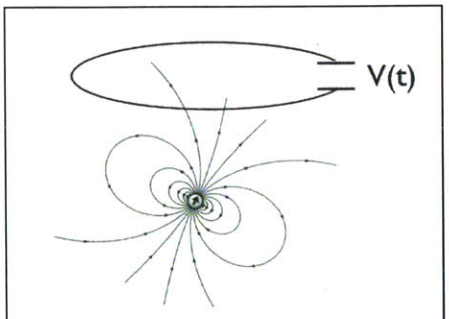

Figure 5 induced voltage in a wire loop due to magnetic field oscillations; Faraday's Law (14)

Excitation

To get a signal out of the system we want to get a "wiggle" out of $\bar{M}$ so that a voltage can be created by Faraday's law of induction. To get this "wiggle" we can apply an oscillating magnetic field, called $\overline{B_1}$, in the x y plane. The source of this oscillating field is the magnetic component of an RF signal. If we simply excite at some random frequency not much will happen, however (this is key!): if we excite at the Larmor frequency the nuclei will start precessing in phase with each other! Now the net magnetization vector $\bar{M}$ is not only in z, but has components in the x y plane because the precessions are going in phase

with each other and the in plane components do *not* cancel. From a mechanical perspective think of the masses in Figure 6 oscillating at the same natural frequency ω_n but at random phases. Now if we drive the base at $\omega_n = \sqrt{\frac{k}{m}}$, the masses will come into phase with each other, and the magnitude will grow.

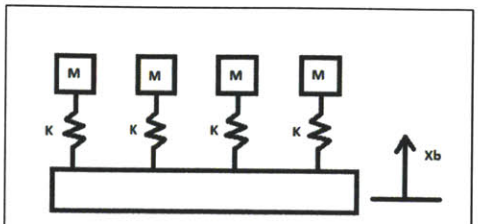

Figure 6

Just as for the B_0 field the rate of change of this new oscillating net field can be expressed as : $\bar{T} = \bar{M} \times \overline{B_1} \quad \rightarrow \quad \omega_1 = -\gamma_p^r B_1$

If B_1 is sufficiently strong and/or long enough in duration $\bar{M}$ can rotate 90°, the z component is gone, and this is called a 90°. pulse. Any rotation angle can be created provided the pulse is sufficiently long and intense.

Relaxation

After the B_1 field is removed (RF pulse), the processions begin to go out of phase again. The x y components of the magnetization vector begins to fade and the M_z component begins to grow again.

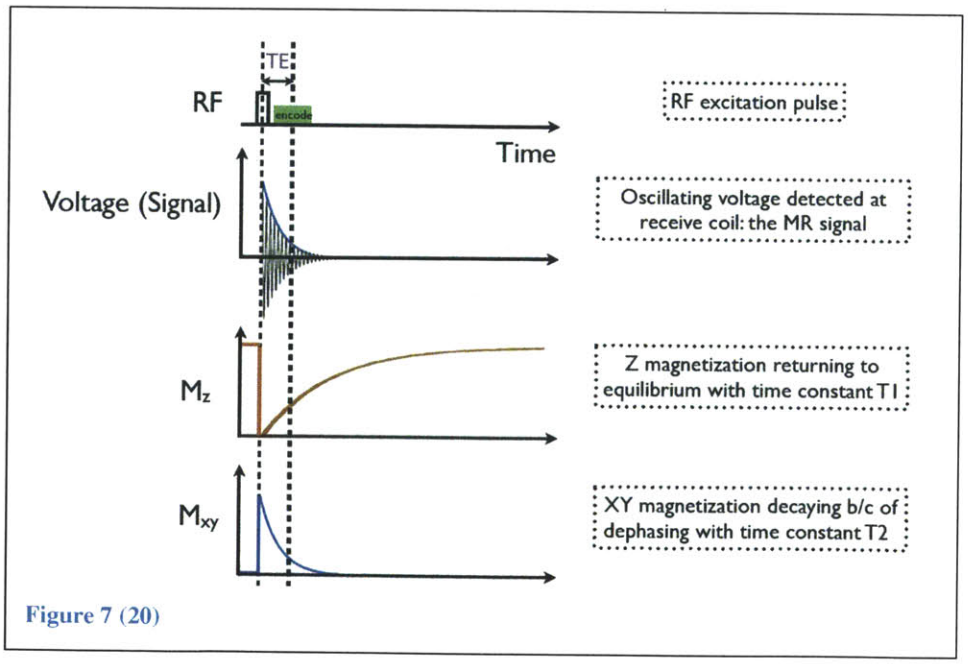

Figure 7 (20)

What we are ultimately after are the T1 and T2 time constants that describe the envelope of signal decay as the nuclei de-phase and settle back to the B_0 direction after excitation (among other measures such as proton density). T1 and T2 are tissue dependent and are what give the MRI image contrast and allow tissues to be differentiated. The receiving coils pick up this free induction decay or FID signal.

Encoding Space

The key to encoding space in MRI is the Larmor frequency's linear dependence on magnetic field strength. A magnetic gradient G_z, in the z direction, can be applied on top of the very strong B_0 field so that the Larmor frequency of the nuclei is linearly dependent on the Z

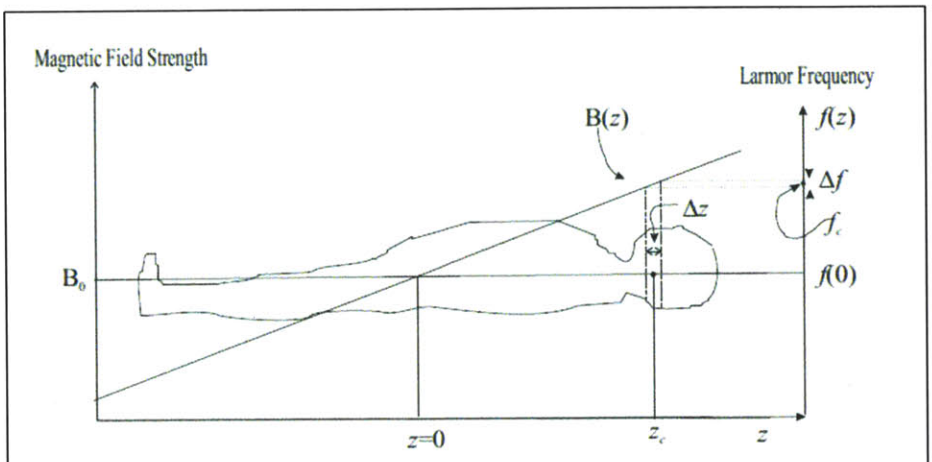

Figure 8 (14)

position. We can excite "slices" in the z direction with location and thickness determined by the center frequency and bandwidth of the RF excitation pulse defined by:

$$\Delta f = \Delta z G_Z \gamma_P$$

Similarly to encode position in the x direction we can apply another magnetic gradient G_X in the x direction. So the Larmor frequency for a nucleus with X and Z coordinates is:

$$\omega = \gamma_P B_0 + \gamma_P G_X x + \gamma_P G_Z z$$

So in general the FID signal coming from a selected "slice" is:

$$s(t) \propto \iint_{x\,y} m(x,y) e^{-j\,\omega(x,y)t}$$

Where $m(x,y)$ is the decay envelope of the FID signal. Position encoding in the x and z directions is called frequency encoding.

To encode position in the *y* direction *phase* encoding is used. To encode phase in the *y* direction an 90° RF pulse is applied, as the precessions begin to de-phase, a gradient G_y , in the *y* direction is switched on for time τ. This imparts an in phase precession in the *y* direction which varies linearly in *y*. When G_y is switched off the spins go back to their *x z* precessions but maintain a linear de-phasing from the G_y pulse. A 180° pulse is then applied which *without* the *y* pulse, would reverse the random de-phasing and bring all the spins back into phase in the *x y* plane. However with the G_y pulse, the spins maintain their *linear* de-phasing after the 180° pulse. After the 180° pulse the spins are encoded in the y direction by their phase shift. The phase shift acquired is described as:

$$\varphi(y) = \int_0^{\tau} \omega(y)dt = \omega\tau = (\gamma_P y G_y)\tau$$

Including this in our FID signal we have:

$$s(t) \propto \iint_{x\,y} m(x,y)e^{-j\,[\gamma_P z G_z + \gamma_P x G_x + (\gamma_P y G_y)\tau]}dydx$$

Thus the frequency of the FID signal received from each spin is a function of *x y and z* position and the applied magnetic gradients. Thus each *x y z* region has its own unique frequency and corresponding envelope of decay *m(x,y)*. An inverse 2^d Fourier transform can be applied to recover this *m(x,y)* magnitude which gives that *x y z* region, or voxel, an intensity.

Some things that affect image quality in MRI are the Homogeneity of the B0 field and spatial homogeneity of the B1 field. Effects from eddy currents also interfere with the applied fields; these eddy currents can be generated on any conductor in the magnet bore. Changes in magnetic susceptibility can induce magnetic gradients which distort the applied fields; this effect is increased with field strength. Lastly Brownian motion of the water protons contributes to thermal noise.

2. Design of the 7T 32 channel ex vivo coil assembly

2.1. Fundamental Requirement Overview

The main requirements of the ex-vivo scanning assembly are:

1) Position the brain and all associated transmitting/sensing electronics at the iso-center of the 7T magnet bore

2) Contain the brain in a re-sealable vessel for scanning and storage

3) Place the receiving coils as close to the brain as possible for high resolution images and

4) Do not distort or damage the brain tissue. Additionally, air bubbles cause artifacts during imaging and must be removed in a separate process.

2.2. Previous Approaches

All previous work was carried out at the Athinoula A. Martinos Center for Biomedical Imaging **(3)**

2.2.1. Previous Holder Design

One previous brain holding approach involved a molded fiberglass shell and flat plate lid as shown in Figure 9. A degassed brain sample, sealed in a bag, is placed in the shell for scanning. One difficulty with this approach is the lack of features on the shell to aid the receiving coil layout as discussed in 2.2.3. Receiving coils must be tessellated over the surface of the shell and this design requires a tedious trial and error process to position the coils. Bunching of the brain bag also poses a problem when imaging due to changes in magnetic susceptibility at the liquid, bag, and air interfaces. Another challenge in this design is the lack of a rigid, cohesive mechanical structure to support the electronic components.

Figure 9

Another previous approach to holding the brain was a 3d printed holder that conformed to the brain (Figure 10). This design had two main drawbacks: 1) the fused deposition printing process resulted in a porous structure that was not air or liquid tight leading to leaking PLP preservative 2) while the holder

conformed nicely to one brain, the high variability in brain size rendered the holder less useful with other brains.

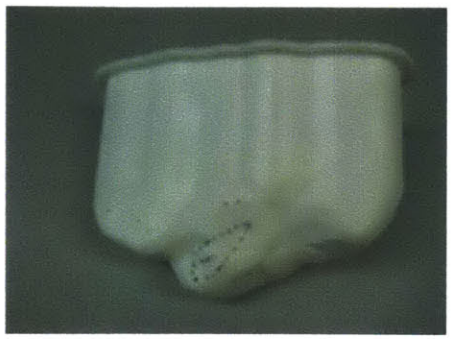

Figure 10

2.2.2. Previous Birdcage Design

The "birdcage" is a cylindrical array of RF coils that transmit the B1 excitation field. The "birdcage" surrounds the sample and receiving coil array and is concentric with the B0 magnet bore. Previous successful designs employed a large cast acrylic tube onto which the transmitting coils were laid. Figure 11 below shows a previous design. The longitudinal and circumferential copper strips are the transmitting coils.

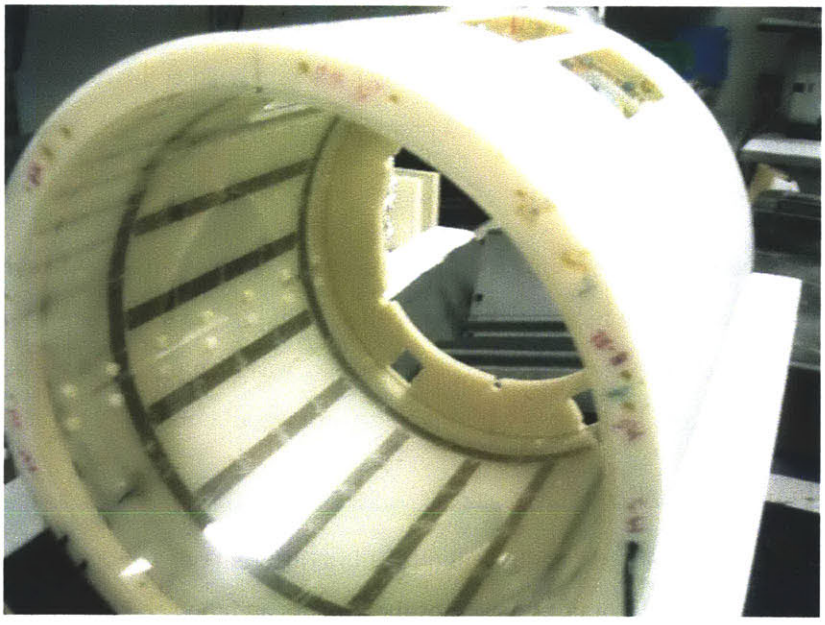

Figure 11

2.2.3. Previous Receive Array Design

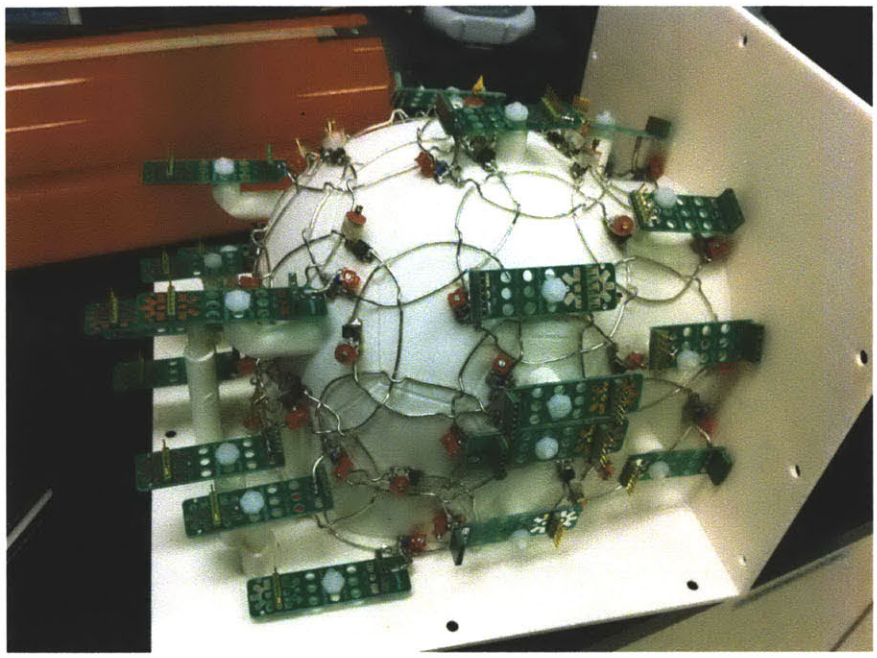

Figure 12

Recent head receive coil from Martinos group

The receive array former in this work builds on the most recent array designs from the coil building group at the Martinos center. Figure 12 shows a recent head coil with a 3d printed former that includes the hexagonal coil layout features and preamp standoffs.

2.2.4. Previous Degassing Approach

The previous degassing method was to submerge the brain in PLP solution in a heat-sealable bag, then massage and tap the brain to remove bubbles. The air collected at the top of the bag was then sucked out with a needle and syringe and the bag resealed. The sealed bag was then placed in the scanning apparatus. The process proved to be lengthy and unable to remove all bubbles.

2.3. The Manufacturing Challenge

The ex-vivo coil assemblies are one-off, each design fulfills a different need or is an iteration of previous work. They are built in lab; the exploratory nature of the process and the need to iterate demands flexible,

low cost, and rapid manufacturing methods. Shipping work out to other shops is often difficult because of the need to rapidly make changes during the building process or to quickly implement new ideas.

2.4. The Manufacturing Solution

In this project a unique set of existing and newly developed tools are brought together to enable less expensive development of ex-vivo coils and to enhance the existing build capabilities. These manufacturing tools and design methods are intended to provide the flexibility and capability to produce components with increased accuracy and improved properties while expanding the limits of what is possible to build in-lab. Increasing coil building ability opens the possibility of developing a wide range of custom coils to improve all MRI imaging.

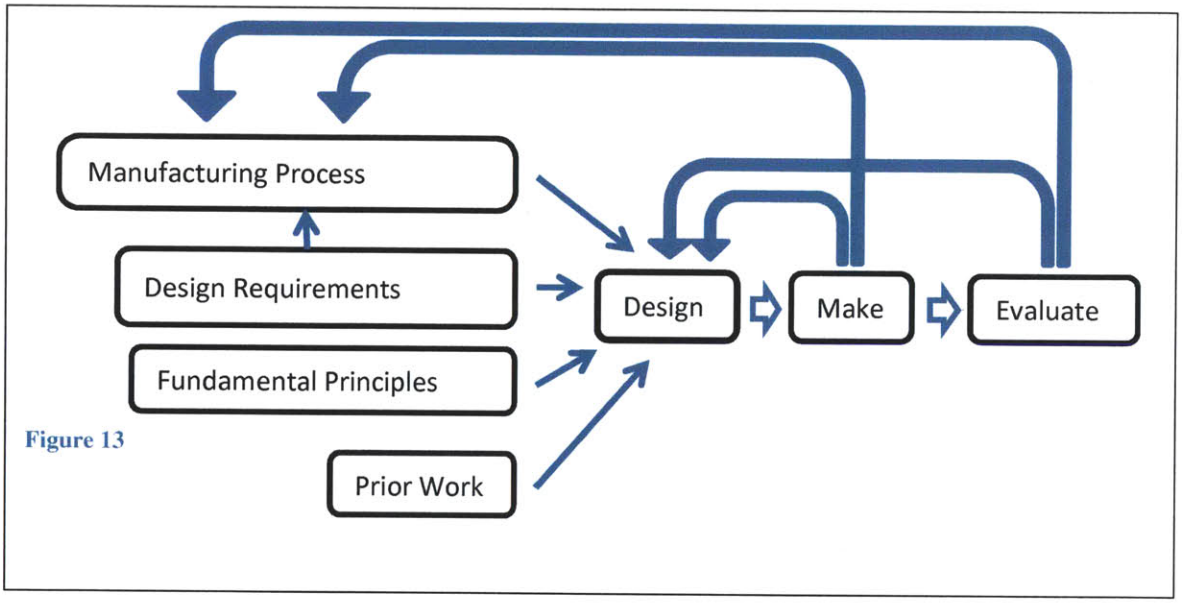

Figure 13

Figure 13 shows the general flow of concepts and processes in the design and construction of the ex-vivo assembly. Most important is how connected and fundamental the manufacturing methods are to the design. Many of the challenges associated with the ex-vivo coil design are manufacturing related and an important aspect of this work is the closed loop from *manufacturing process →design →make* and back around. The solution not only requires a product design but also a concurrent process design as well.

2.5. Design Overview

This thesis presents the mechanical design and construction of a 32 channel 7T array. All electrical design and construction is carried out by members of the Martinos MRI coil group who have been designing and building coils for over 10 years. In the new design of the 32 channel ex-vivo brain holder (shown in cross section in Figure 14), some innovative design features and processes have been implemented to address the design requirements and limitations of previous iterations. The underlying

structure of the 32 channel coil is based on a stiff, protective, cohesive chassis that minimizes the length of structural loops. This chassis or frame provides alignment and reference during assembly, and a structural "ground" for component and subassembly mounting. The design is composed of a series of concentric rings, connected by stringers, into which a skin is bonded forming a tube for the transmitting array. This design is very similar to airplane fuselage construction and results in a stiff, well aligned, low cost structure. "Formers" are used to describe the mechanical structures for the transmitting and receiving coil arrays because they form the coils to the proper geometry.

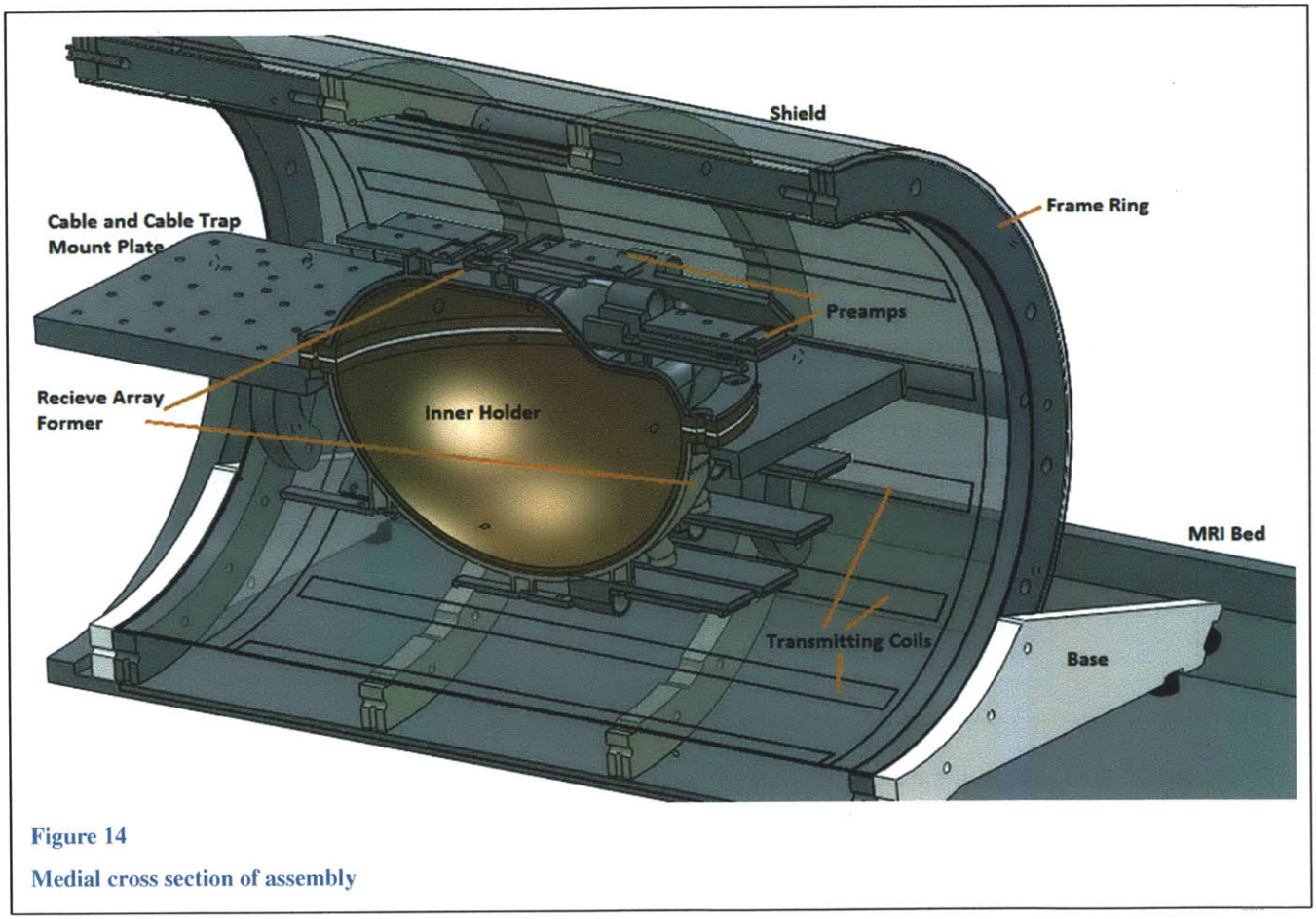

Figure 14
Medial cross section of assembly

2.6. Detailed Requirements and Design Solutions

The design requirements of the ex-vivo brain scanning assembly are: 1) Position the brain and all associated transmitting/sensing electronics at the iso-center of the 7T magnet bore 2) Place the receiving coils as close to the brain as possible for high resolution images 3) Contain the brain in a re-sealable vessel for scanning and storage 4) Do not distort or damage the brain tissue 5) air bubbles cause artifacts during imaging and must be removed in a separate process. Figure 15 shows the completed scanning assembly.

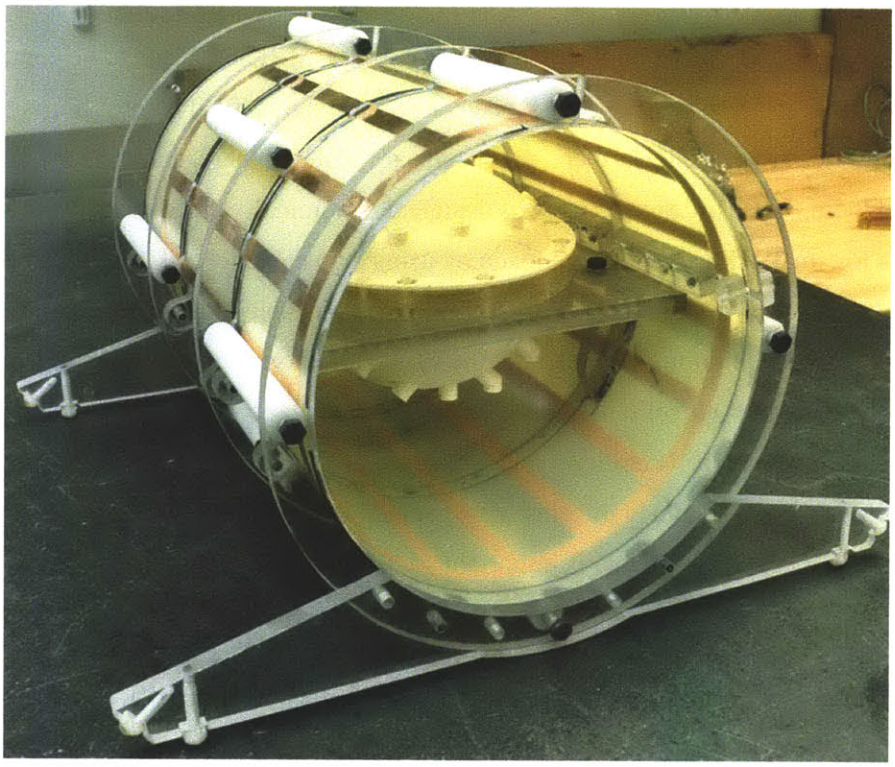

Figure 15

Mechanical assembly of 32ch. 7T array

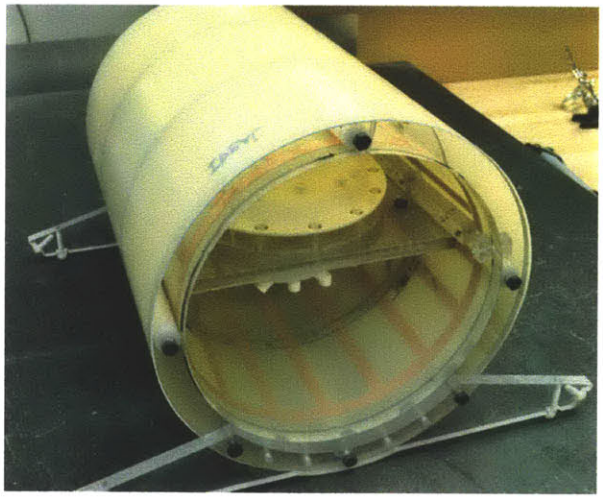

Figure 16

Assembled with shield on

Requirement 1: Positioning

The ex-vivo coil assembly is placed on the patient bed of the 7T MRI and needs to be centered in the magnet bore. The brain must be positioned at isocenter because the B_0 field is most homogenous there, the $G_{x,y,z}$ gradient fields are most linear there, shim coils are centered there, and the RF transmitting coils must be centered there. The Birdcage frame was designed to nominally place the brain at isocenter and accommodations for small adjustments were made by using adjustable feet. The base is designed to use 3 non-parallel planes on the MRI bed to provide a unique and repeatable mounting orientation. The primary reference is the bed bottom, secondary is the vertical back wall of the bed, and tertiary is the side wall on the bed. The number of feet required for each reference plane would be 3,2,1 if mounting were exactly constrained. However, for stability 4 feet were used on the primary reference. In this work it is not often that high positional accuracy dictates since each system is tuned to achieve desired electrical properties. Rather, it is repeatability that is important so that these tuned parameters remain as such.

Requirement 2: Coil Placement

The shell for holding the receiving coils, known as the "coil former" (Figure 17), fully surrounds the inner holder and serves as the mounting location for the receiving coils.

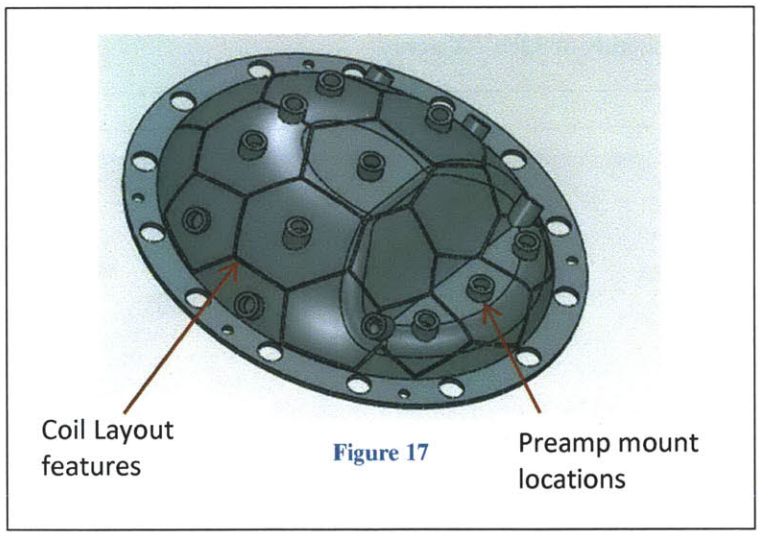

Figure 17

It is composed of two 3d printed shells. 3d printing was selected due to the complex geometry and need for only one set. The receive array is really the heart of the ex-vivo assembly and once built and tuned will not change and is sized to accommodate a limited range of brain sizes as discussed in 0. An array of 31 copper coils, each with a passive pre-amplifying circuit, must be tessellated over the surface of the brain. The closer these coils are to the surface of the brain, the better the signal to noise ratio. The close proximity of the coils to the brain is the motivation behind ex vivo imaging as opposed to in vivo. The

coils all have overlap with their neighbors as shown in Figure 18 to cancel out mutual inductance between nearest neighbors. Figure 18 shows the 3d printed receive former, a preamplifier, and the receive coils.

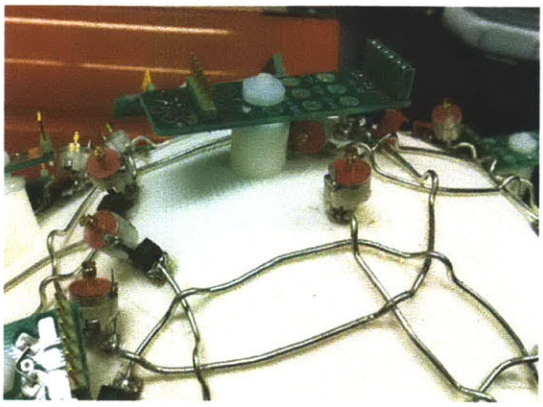

Figure 18

Close up of receiving coils with preamps all laid out on 3d printed former

To guide the coil placement during assembly, a pattern of hexagons and pentagons were tessellated over the surface of the top and bottom coil former. Symmetric, evenly sized hexagons and pentagons were tessellated over the former surface in SolidWorks, details of the process are presented in Appendix A. These shapes were embossed on the 3d printed formers and dramatically speed the coil construction process by providing a layout template (4).

Receiving coils are tuned for one specific geometry, repeatability of coil alignment is important for consistent performance. Coupling between the coils is a function of the separation. Combined signal across all coils is strongly dependent on how correlated the noise is between the elements. To ensure repeatable alignment of the former halves in the XY plane a locating pin and stop were used. The pin is fixed to the bottom receiving former and passes through a close fit (.004" clearance) hole in the upper receiving former. This provides a constraint in the XY direction and eliminates two of the three degrees of freedom in the XY plane. A stop is the used to fully constrain the holder in the XY plane by removing the rotation DOF. Figure 20 shows the pin location as it acts as a rotation origin.

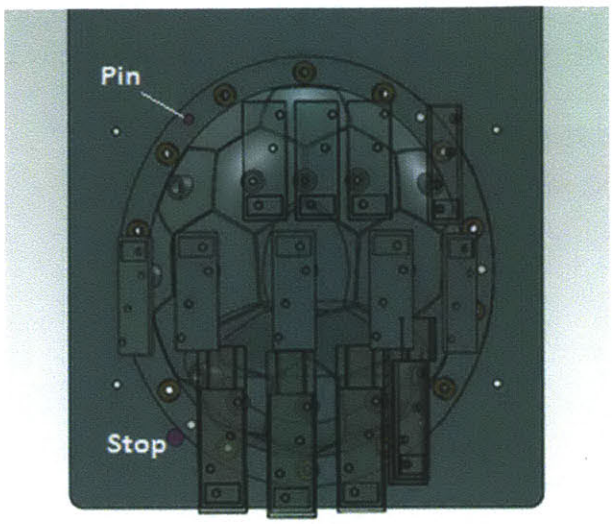

Figure 19

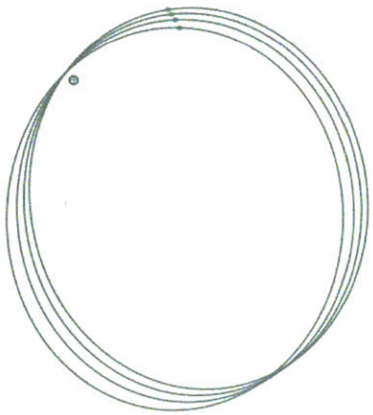

Figure 20

possible rotation displacements with pin only

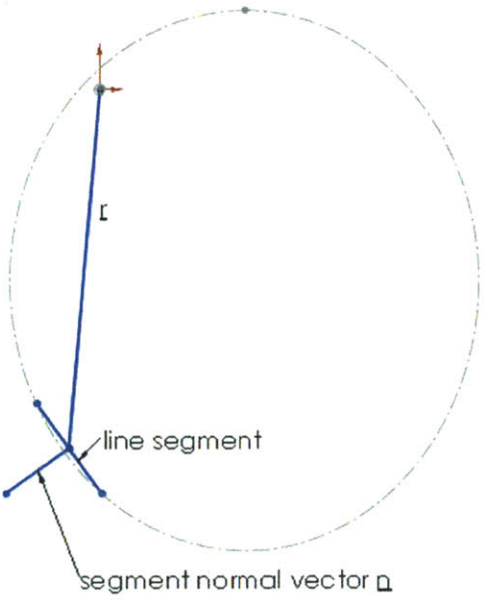

Figure 21

To find the most effective location of the pin, start by considering the direction of the force reaction between the pin face and surface of the part. Vector $\underline{r}$ is from the rotation center (pin center) to the pin/ part contact location, θ is an angular displacement, $\underline{n}$ is the unit normal vector for the contact point on the part, and F_n is the normal force reaction. For the greatest constraint stiffness we desire the moment about the origin created by F_n to be maximized

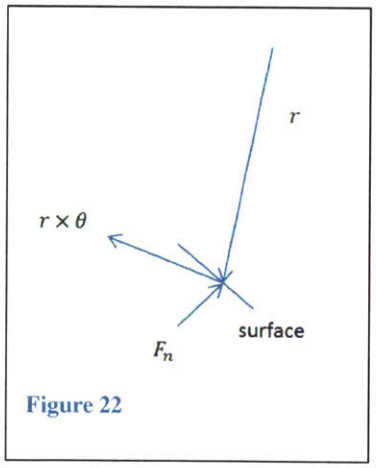

Figure 22

$$F_n = n \cdot (r \times \theta) \rightarrow \theta \cdot (r \times n)$$

The sensitivity of the constraint force to rotation is:

$$\frac{\partial F_n}{\partial \theta} = r \times n$$

It is desirable to maximize this sensitivity for the greatest rotation constraint

To find the optimum rotation constraint location the perimeter geometry of the upper former bolt flange was extracted from CAD into a data file using DanCam, then a Matlab script carried out the $(r \times n)$ operation for all line segments forming the perimeter. Figure 23 shows the results graphically and pinpoints the ideal rotation constraint location.

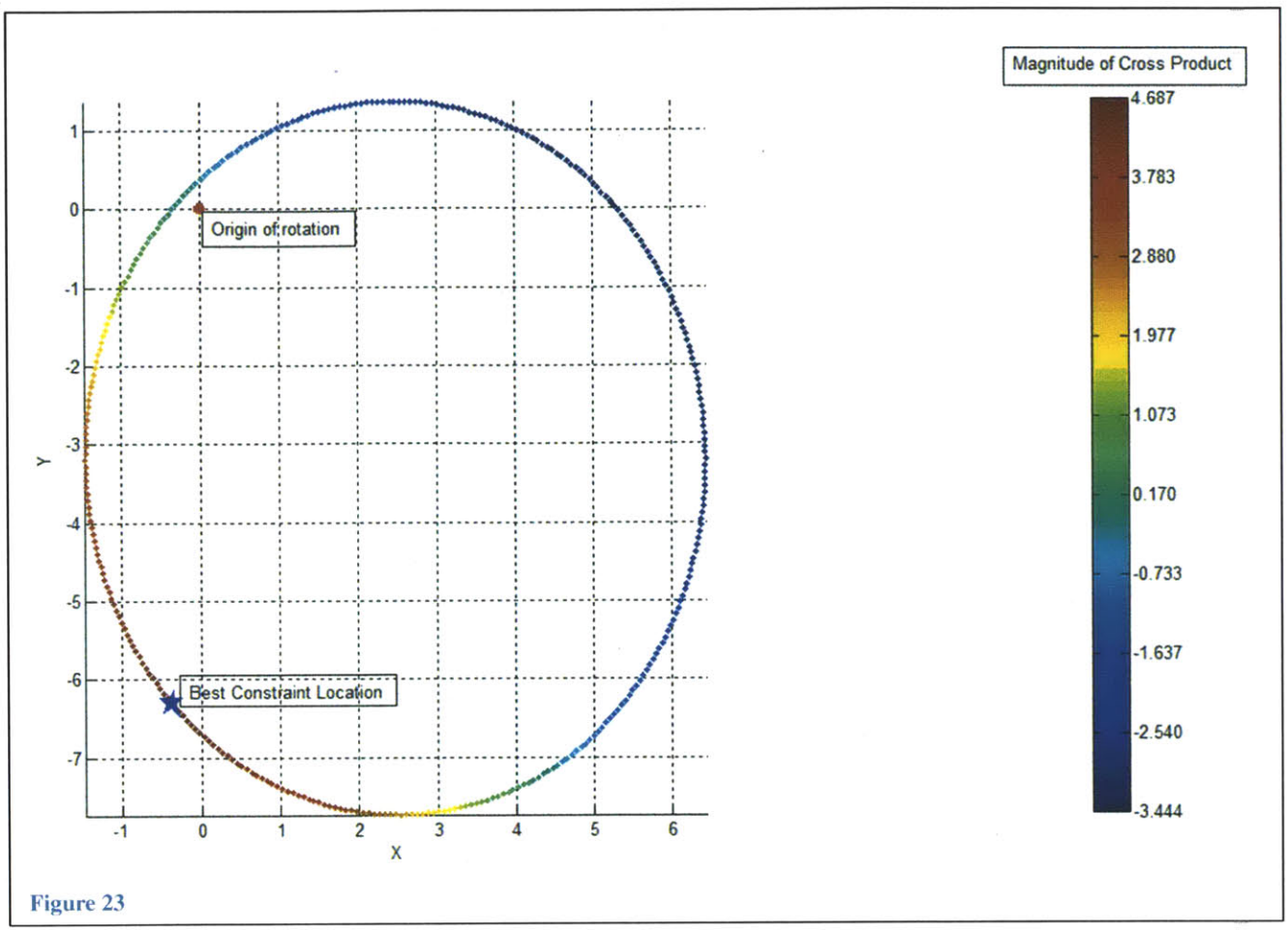

Figure 23

Requirement 3: Brain Housing

A re-sealable container for the brain is needed because it prevents the degased brain from coming into contact with air and submerged in PLP. It also keeps the toxic PLP solution away from the rest of the ex-vivo assembly and eliminates human contact with the solution, this allows the brain to be safely handled and stored outside a fume hood. Each brain will be stored and degassed in its own "holder" which can be neatly and easily swapped out of the scanning assembly. Several of these holders were required and had to meet the following requirements: long term chemical resistance, liquid and gas tightness, two ports to accommodate the degassing process, ability to withstand 29.5"Hg vacuum pressure, see-thru, and durable. Due to the specific material requirements and the need for multiples, a substantial effort was put into developing a bench top vacuum casting system discussed in Section 3.

To address the chemical resistance, clarity, and casting requirements (low viscosity, low shrinkage, adequate gel time) Epon 315C epoxy was selected for initial prototypes. 3 months of continuous exposure to the PLP solution revealed no changes in the material such as softening, pitting, discoloration,

or cracking. The highly cross-linked epoxy combined with the ability of vacuum casting to produce void-free parts allowed for gas tight holders. Repeated pressure testing validated the designs suitability to withstand atmospheric pressure under full vacuum. However the Epon 315c and Epikure 3234 curing agent proved to be somewhat brittle and less durable than desired.

To address the poor toughness of the epoxy cast holders, a new set were cast using a rigid polyurethane (Freeman 1090) with a Shore hardness of 80 and a flexural strength of 11,000Psi and a .1% shrinkage and 600 centipoise mixed viscosity. The finished urethane holders proved to be far tougher and able to withstand accidental drops. No data could be found on PLP chemical compatibility with urethane so long term compatibility with the PLP fixative will be tested.

Sealing between the top and bottom holder halves is accomplished with a vacuum cast silicone gasket discussed in 3.2.11. Various gasket thicknesses were cast to allow for slight holder volume adjustment to accommodate small variations in nominal brain size. Pockets were included in the sealing flange to reduce material usage and mitigate the effects of shrinkage in the casting.

Figure 24

Holder and holder stand (used for assembly, degassing, storage)

Requirement 4: Brain Holding

The brain holder needs to lightly constrain the brain and position the receive coils close to the surface without squishing, distorting, or damaging the brain. The tissue is fragile and the brains overall shape

must be preserved. There is large variation in brain size and this variation proved to be very difficult to accommodate while satisfying the coil positioning requirements.

Means and Standard deviations for Brain Volume in Cubic Centimeters (5)

	Women	**Men**
Brain volume	$\mu = 1130\ \sigma = 112$	$\mu = 1243\ \sigma = 110$

The brain was approximated as a half ellipsoid with principal axes lengths *a,b,c* where *b=c*. Thus the brain volume is approximated as: $V = \frac{4}{6}\pi\ ab^2$. A rough length to width (*b/a*) ratio of .8 was established from measuring actual brains. Varying the brain volume up and down 1 standard deviation (so 1018 to 1242 for a woman's brain) and solving for *a* and *b* dimensions (using the .8 ratio) yielded a change from the nominal *a* and *b* dimensions of .125" in *a* and .1" in *b*. Thus the holder geometry was designed to allow for this approximate 1 standard deviation larger brain.

Adjustable volume holders are not possible because once built, the receiving coil geometry is set. It is a delicate and lengthy process to adjust and tune the properties of the receiving coil in harmony with the transmitting coil for optimal performance. An adjustable holder does no good when the receiving coils can't be adjusted as well.

Requirement 5: Integration with Brain Degas Process

The development of an improved brain degasing method is very important to improving ex-vivo scanning. Trapped air in the brain causes large blooms, or dark spots in the final image due to susceptibility gradients at the liquid/ air interface. The holder is integrated into the degas process; it serves as the low pressure vessel in which the degas process takes place and maintains an air-free, preservative-filled environment for the brain during storage. This meant that the holder must withstand the degasing processes including large amplitude vibration and external pressure when under vacuum. Degasing techniques and results are discussed in section 5. Two fittings are installed on the holders for the degas process, one is a vacuum port and one allows for fluid filling.

2.7. B1 Transmitting Coil Design, The Birdcage

2.7.1. Transmitting Coil Function

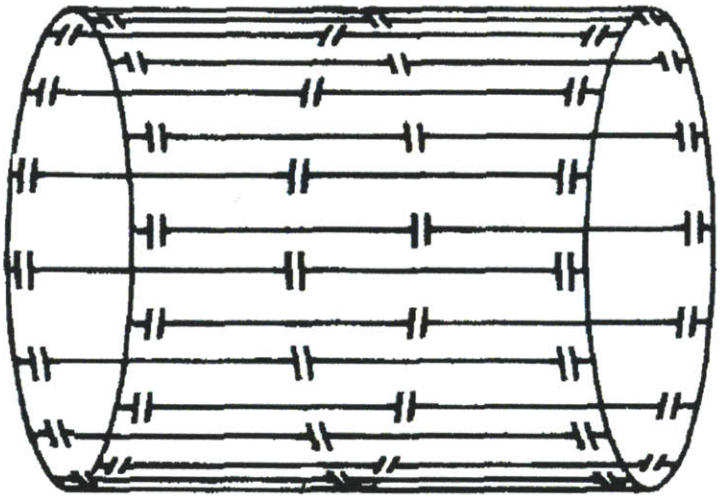

Figure 25

Birdcage style transmitting coil schematic showing conductors and blocking capacitors

Transmitting coils create the radio frequency B1 excitation field that bring the Hydrogen nuclei precessions into phase. Although several different coil styles exist, this particular style is called a birdcage coil. The birdcage forms a series of conductive loops connected in parallel that surround the sample. These loops are fed RF pulses directly from the MRI pulse sequence generator. 16 axial "legs" create 16 loops, the more loops, the more homogeneous the B1 field is. However more conductor area must be balance with the need for the birdcage to remain transparent to RF flux **(6)** and assembly effort. Sixteen legs has been determined to provide adequate homogeneity. Detailing the theory behind RF coil function is beyond the scope of this paper, for more information see **(6)** and **(7)**. Birdcage coil design was guided by research staff at the Athinoula A. Martinos Center for Biomedical Imaging **(3)** who have been constructing coils for 10 years and have extensive coil building experience **(4)** .

Geometry requirements

Testing revealed that B1 field intensity begins to fall off beyond the central 60% region of the coil. Thus the entire receiving array (19cm maximum dimension in the Z direction) needed to be inside this 60% region of the birdcage; this translates to a 32cm electrical length (measured from outer edge to outer edge of the circumferential end coils). 2 cm were added to either end for safety resulting in a 36cm total electrical length. The 10.25" diameter of the birdcage is the maximum possible diameter for the birdcage

while still remaining coincident with the main magnet bore. Any larger and the birdcage would interfere with the MRI patient table.

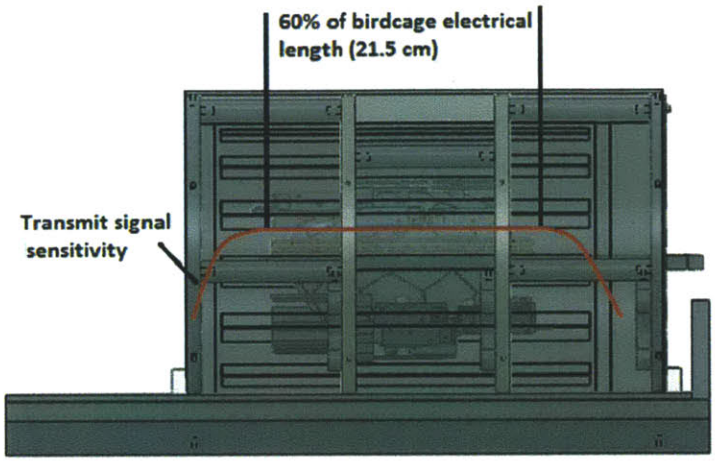

Figure 26

2.7.2. Birdcage Design

As the gradient coils are pulsed, large magnetic fields create eddy currents in the birdcage conductors. These eddy currents in turn produce perpendicular Lorenz forces. The larger the conductive strips are, the larger the eddy currents are and in turn generate larger Lorenz forces. These Lorenz forces oscillate with the gradient pulses and can cause the skin of the transmitting coil to vibrate **(8)**. To reduce eddy currents conductors are kept narrow (0.5" in this design). Further eddy current mitigation is provided by blocking capacitors on the axial and circumferential legs of the birdcage. These capacitors are tuned such that they act as an open at low frequencies which are associated with eddy current formation; this further minimizes the area available for eddy current formation. At the high operational frequencies, the capacitors act as shorts and do not impede function. Figure 28 shows a unwrapped segment of the transmitting coil note the blocking capacitors.

Figure 27

The birdcage sheet laid flat with installed conductors

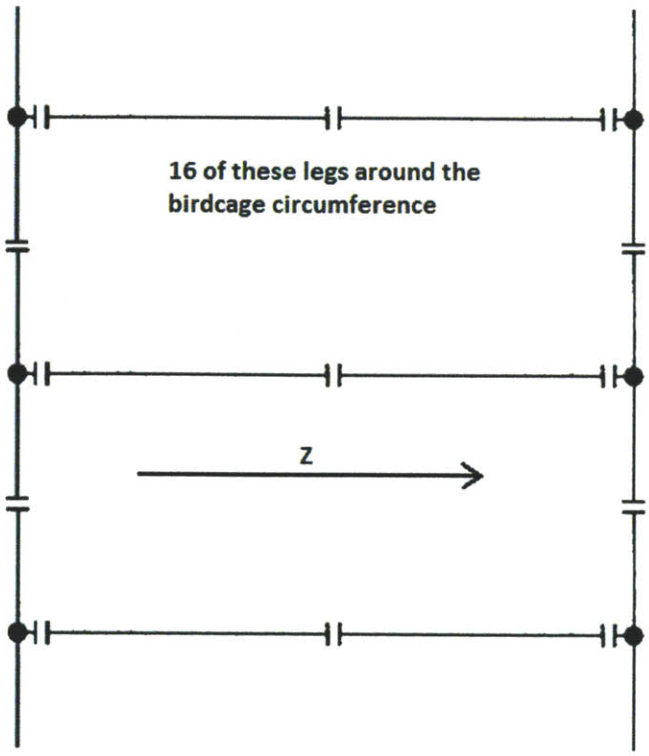

Figure 28

Schematic of a section of Birdcage Coil

The coils are constructed by laying strips of copper tape in very specific geometries on the tube surface then coupling breaks in the strips with capacitors. Using NC controlled equipment to cut the sheet allows accuracy in positioning the conductors which leads to better performance

Material requirements

The birdcage structure has to be electrically insulating, RF and MR transparent. Typically the birdcages are based on cast acrylic tubes. FR4 fiberglass has also been used in previous designs.

Sheet tube

The required diameter (10.25") was not available in any acrylic or polycarbonate tube; thus the shape and structure of the birdcage had to be created another way. Several options for creating the tube were considered which are outlined in Table 1.

Method	Advantages	Disadvantages
Molded fiberglass with vacuum bag	Very stiff, continuous, free of residual stress	Poor bag-side surface, dimensionally accurate mold needs to be constructed
Molded fiberglass with matched molds	Very stiff, continuous, free of residual stress, good surface inside and out	Mold has to be strong, dimensionally accurate, able to remove part
Casting	Good surface on both sides, mold has less mechanical req's than fiberglass mold	Low strength, unknown resistance to thermal fatigue, low heat resistance
Rolled Sheet	Excellent thickness tolerance and surface finish, wide variety of materials available, cutting and shaping can be done flat with NC equipment, low cost, no mold required	Requires frame to ensure dimensional accuracy

Table 1

It was decided to replace the cast acrylic tube with a sheet material having several advantages: wide selection of materials and thicknesses, low cost, and the ability to lay the sheet flat for cutting (laser, water jet, or by hand) and the laying of transmitting coils. The sheet was designed in SolidWorks as a sheet metal-type part with a bend radius equal to the birdcage radius. This allowed all the cutouts and feature to be placed with the sheet in a rolled configuration within the entire assembly, then "un-rolled" or laid out as a flat part which could be converted to a DXF file to easily and precisely cut the sheet on a waterjet. This ease and precision is not possible with a round tube and conventional waterjet. This method also allows future designs to use copper clad FR4 sheet then have the coils and electrical features routed out for enhanced precision.

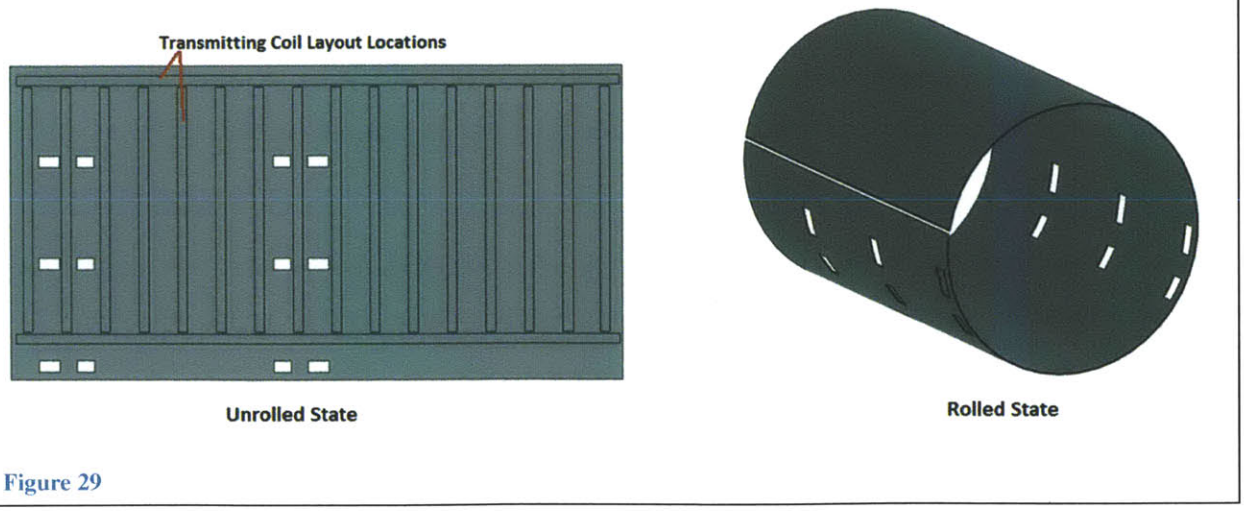

Figure 29

The "seam clamps" in Figure 30 are critical to making the sheet design work, especially in stiffer materials like FR4. These clamps have surfaces matched to the curvature of the birdcage and bridge the seam in the sheet. When tightened they force the edges of the sheet to be tangent. Without these clamps the sheet will take on a teardrop shape. Because the clamps bridge the seam gap, much "looser" tolerances can be used for the sheet width, whereas prior to the seam clamp the sheet width had to nearly exactly match the inner circumference of the frame rings. As the clamps are tightened down the sheet will adjust its circumference to exactly match the frame ring similar to how a rolled poster will expand radially inside a poster tube until it matches the tube diameter.

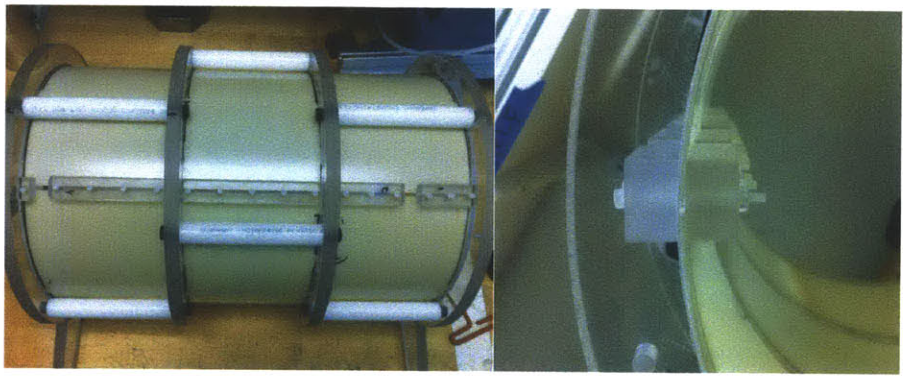

Figure 30

Seam clamps enforce tangency at sheet seam

Birdcage Frame

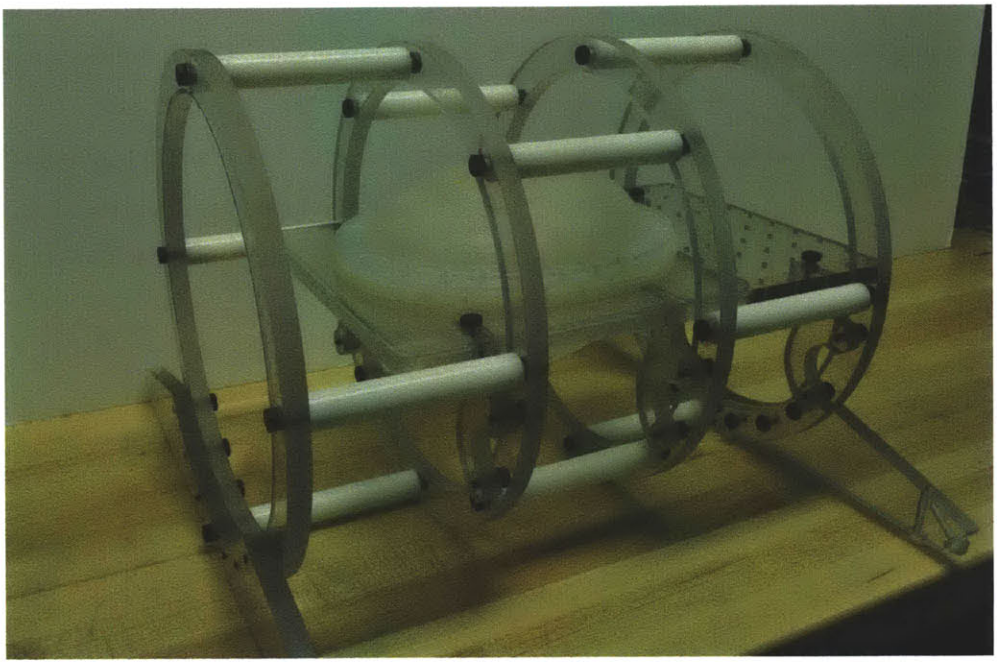

Figure 31

Bare frame without transmitting surface or shield, cable mount plate and inner holder

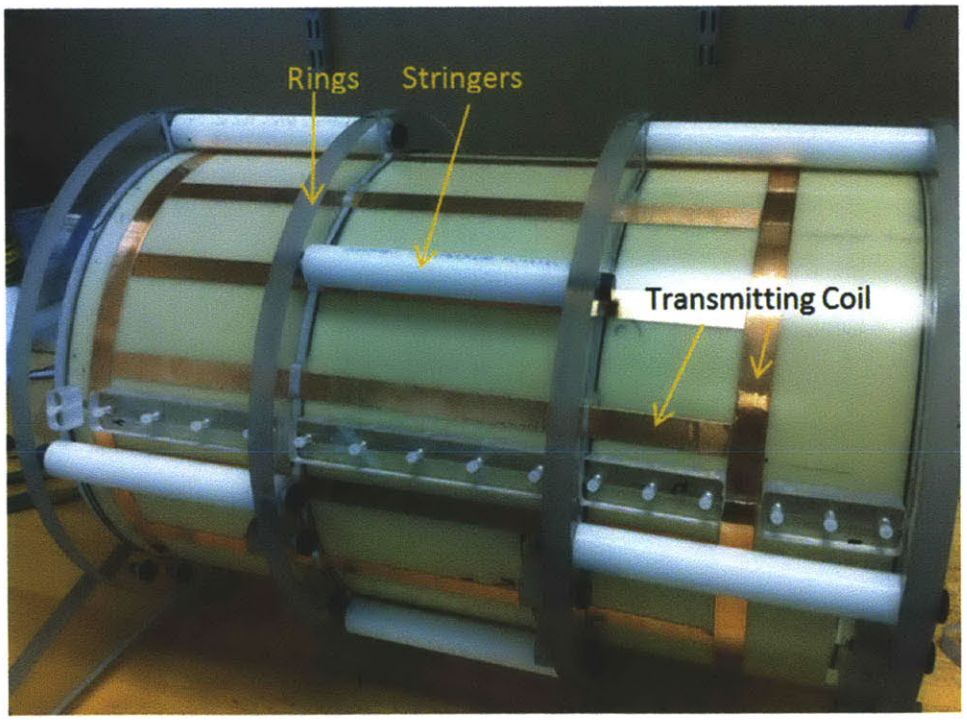

Figure 32

Frame with transmitting sheet and coils rolled and inserted

To accommodate the rolled tube concept a ring and stringer style frame was developed. The concept for the frame is to provide a rigid, well aligned structure to provide a mounting template for the transmitting sheet. The frame itself is based on a series of 2d geometries each occupying they're own plane in the axial or Z direction of the birdcage. These planes are joined by stringers which provide axial alignment and spacing. The rings provide diametral stiffness and sheet constraint, the stringers provide axial stiffness and constraint. The birdcage is assembled by rolling the transmitting coil sheet (having been cut and coils laid out) and positioning it in the frame, bonding the sheet into the frame completes the structure.

Bolted joints are advantageous for providing damping due to energy dissipation from friction at the joint interfaces. Glass filled plastic fasteners were used throughout the assembly. This approach proved to be successful as shown by the results plotted in Figure 33. Figure 33 represents one of the quality assurance measures used at the Martinos Center. The abscissa represents sample number, the ordinate is average signal intensity from a group of voxels located at the center of a gel phantom brain. Ideally the intensity would be constant for all samples since nothing is changing, but due to mechanical and electrical disturbances, the signal varies. The white signal is actual, the green is de-trended to remove the effects of thermal drift, the blue line is a best fit trend line. A peak to peak (P2P) value of .5% is desired, the birdcage tested here achieved a P2P of .48%. This low variation in signal intensity is attributed to the structures stiffness and high damping.

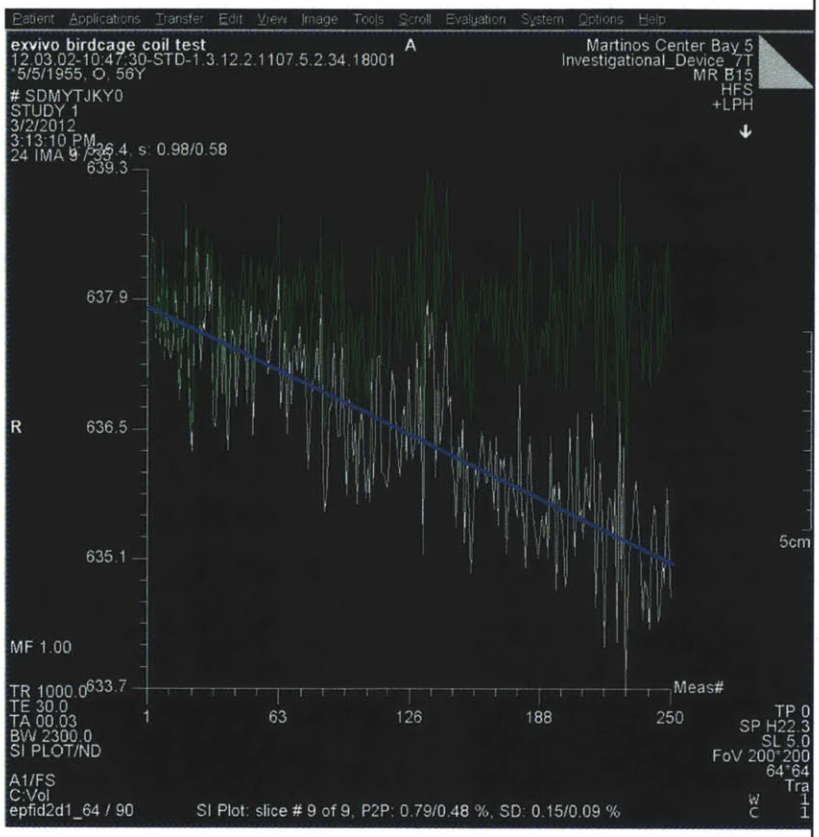

Figure 33

Stability plot with phantom. Trend line in blue thickened for visibility

2.7.3. Mounting Plate Subassembly

The concept behind the "mounting plate," shown in Figure 14 is to keep the receiving coil array, cable traps, cables, and additional electronics all solidly mounted to a single piece that can be removed and inserted into the birdcage as needed. The receive array sends signals from each of its 31 coils to passive preamplifiers, receivers for analog to digital conversion to RAID data storage for later post-processing. The ex vivo assembly is connected to peripheral equipment thru large diameter shielded cables which are permanently mounted to the mounting plate on one end and terminate with large connectors on the other. This subassembly concept prevents relative motion between the receive array, receive signal conditioners, MRI cables, and MRI cable traps. This eliminates undue strain on the delicate wiring connecting receive coils to signal conditioners and awkward handling during scanning preparations. The mounting plate ties directly to the structure of the main frame providing a solid interface between brain holders and frame. The generic hole pattern at the rear of the plate provides a mounting space for components.

2.7.4. Planar Geometries

Planar geometries are an important and repeating concept in this work because they allow rapid, accurate, and low cost production through the use of advanced manufacturing techniques like laser or waterjet cutting. The advantage of these methods over machining are: little to no clamping / cutting forces, rapid path generation, high speed, and low operator involvement. The advantage of planar parts over 3d parts with respect to 3d printing are: increased precision and dimensional stability, improved mechanical properties, and material choice. Planar geometries can take advantage of the as-manufactured surfaces of plate stock which are often held to tight flatness and thickness tolerances. This is illustrated in the face to face interface between the frame rings and mounting plate brackets.

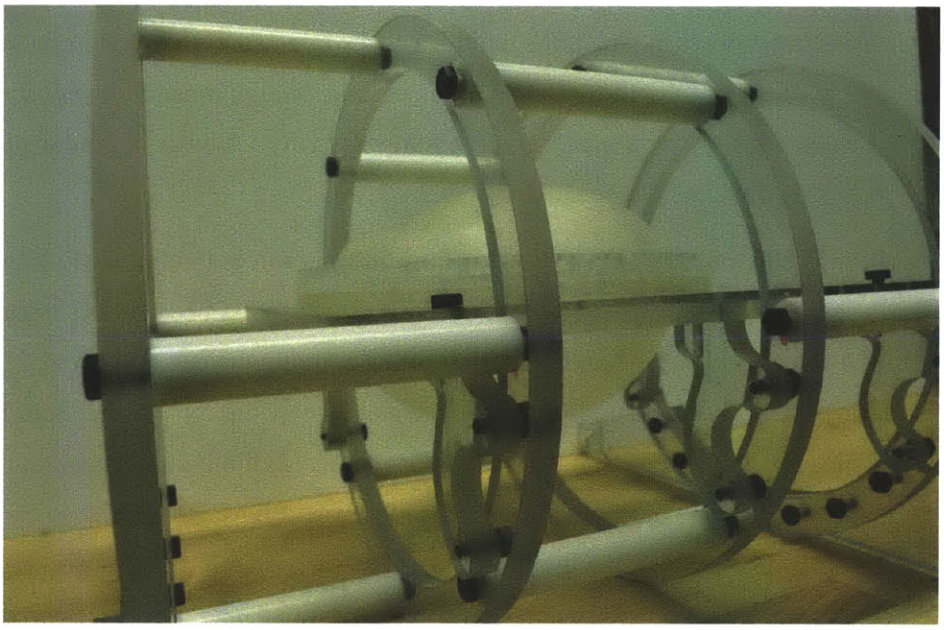

Figure 34

Bare frame showing how flat stock is used in a face-to-face configuration

3. Manufacturing Processes

3.1. Selecting Processes

The main requirements for selecting the manufacturing processes used were: Cost, ability to use the method in a small lab, wide material selection, and time. Successful execution of the design required a set of flexible prototyping tools that are low cost, and leverage common manufacturing capabilities. A major portion of the work was devoted to developing two such tools: the bench-top vacuum casting unit and a computer aided manufacturing program nicknamed "DanCam."

3.2. The Bench-top vacuum casting unit

3.2.1. Process Overview

Vacuum casting is a casting process in which the mold is filled while under vacuum to eliminate porosity and encourage complete filling of intricate molds. During casting the liquid material is pushed into the mold (which is held under vacuum) by atmospheric pressure or gravity. A basic overview of the process is as follows (the process is detailed in Appendix B):

1) The casting material is de-gassed under vacuum to allow buoyant forces to remove dissolved gasses and bubbles. This step is extremely important to the success of the process because any trapped air or gasses in the casting material will cause foaming during filling and ruin the part. Material degassing will be further discussed in 3.2.5. 2) A vacuum is pulled in the mold cavity directly, or the mold is placed in a vacuum chamber. This pressure is important because it controls mold filling rate, forces on the mold, void elimination, and the propensity of the casting material to foam or boil. 3) A valve is opened to allow the liquid casting material to be pushed into the mold by gravity or a differential pressure. 4) After filling the vacuum is released, trapped voids collapse and are completely filled, and the part is cured.

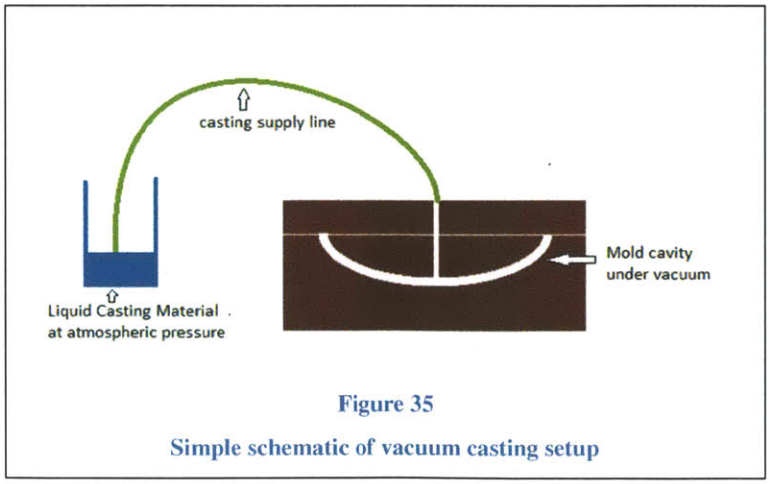

Figure 35

Simple schematic of vacuum casting setup

3.2.2. Advantages of Vacuum Casting

For prototyping of medical devices vacuum casting offers a number of distinct advantages. The largest advantage for this work was the ability to create void free parts. Voids weaken the ex-vivo brain holder, can cause artifacts in the MRI imaging, and may lead to fixative leakage. Void free-parts are due to the absence of entrapped air during casting

The main mechanism for eliminating voids is illustrated by the fact that there is roughly a 150 fold increase in gas volume between atmospheric pressure at 14.7 psi and a casting pressure of .01psi (29inHg). Figure 36 shows how the vacuum casting process is able to effectively fill re-entrant sections of the mold without the need to vent these sections as with more conventional casting processes. After the vacuum is released casting material (resin in this case) is drawn up into the reentrant cavities. With virtually no trapped air to push back on the resin the cavity may be completely filled. Bubbles not removed by buoyant effects during the casting process are essentially squeezed down to a very tiny volume after atmospheric pressure is reapplied.

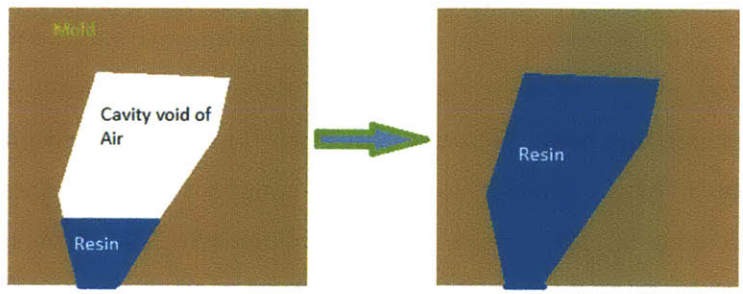

Figure 36

Figure 37 shows a simple experiment demonstrating this filling concept; the tube was filled with air initially with one end held under water and the other end plugged. Everything was placed in a vacuum chamber. When vacuum was applied (29.3inHg in this case) the air expanded and pushed out of the submerged end of the tube. When the vacuum was released water was pushed back into the now void tube almost completely filling it. The tiny bit of remaining air can be seen in the picture, this is all that was left from the full tube of air. Lower pressures could remove more air but were not practical for the vacuum casting because of vapor formation from volatiles in the resin boiling.

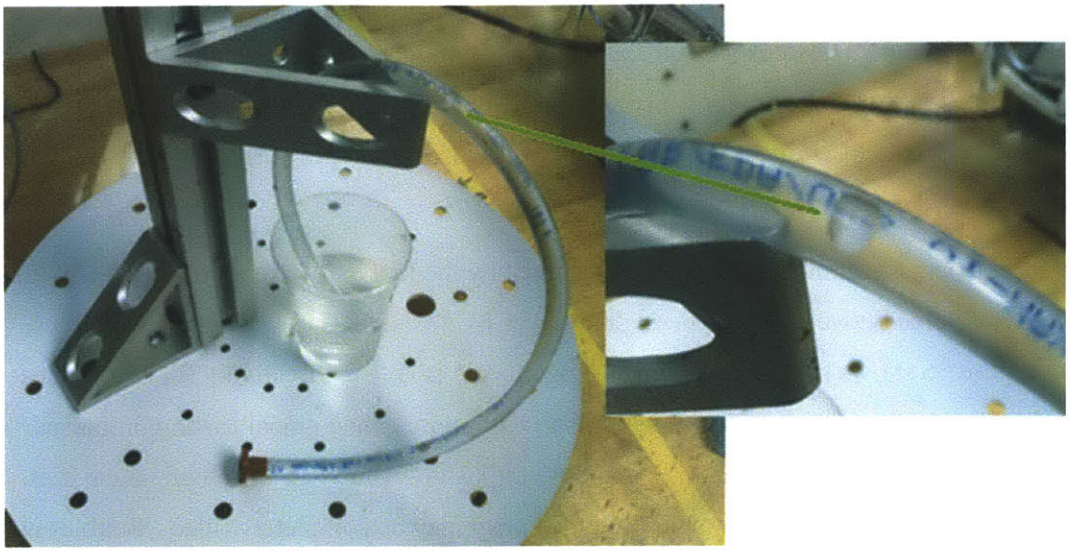

Figure 37

A second major advantage of vacuum casting is the freedom to select any practical material for creating the master model. The material for the master model can be selected for its ease of forming regardless of the material requirements for the finished part. For example machineable wax is relatively inexpensive, can be melted and reused, and is very easily machined. This allows master models to be cut on low stiffness machines with high feed rates. This wax master model is used to create a mold which in turn can be used with any number of cast-able materials that can be optimized for the finished part requirements. Casting uncouples mold material requirements from part requirements. The choice in casting materials is an important factor in many medical devices because of regulatory requirements, stiffness and strength requirements, optical properties, magnetic properties, chemical resistance, bonding properties, etc. Table 2 shows a list of different casting materials for the brain holder.

Material	Flexural Strength (psi)	Tensile Strength	Hardness	Linear Shrinkage	Mixed Viscosity centipoise
Epoxies:					
Epon 815c cured with Epikure 3234 (16)	----------	10,800	85	1%	600
Polyurethanes:					
Freeman 1090 (15)	11,000	2,500	80	.1%	600
Freeman 1080 (17)	9,500	6650	80	.1%	150

Table 2

3.2.3. Benchmarking

Typical vacuum casting machines are large and expensive. The goal in this project was to create a small, low cost desktop unit to fulfill most of the functionality of the larger more expensive units. Renishaw is the primary manufacture of these machines. The units are quite large; the smallest unit is their 5/01 model and measures 1.175 x 1.2 x .594 Meters. Additionally this unit is out of the range of labs and small prototyping firms that could make use of this technology. These units have one open chamber; the casting material is mixed and poured from the upper chamber into the mold which is positioned on an adjustable pedestal in the lower section of the chamber. The whole process takes place under vacuum and the casting material is pulled into the mold by gravity alone. Higher end units like the 5/04 have two separate chambers and can use a pressure difference between the two to force the casting material into the mold, very similar to the desk top unit presented in this work.

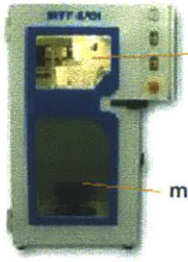

Figure 38

Renishaw 5/01 ULC (18)

3.2.4. The Desk Top System Concept

The basic system shown in Figure 39 is composed of a vacuum pump [1], vacuum chamber [2], resin supply pot [3], resin flow control (hidden from view) [4], resin pot vacuum supply [5], resin supply line [6], and the silicone mold and vented risers [7]. The pump [1] pumps down the chamber [2] and can also supply vacuum to the resin pot for degassing or to control the pressure differential between the resin pot [3] and the vacuum chamber [2]. After casting pressures are achieved, the resin flow control valve [4] is opened and resin flows into silicone mold [7]. The vent tubes coming out of the top of the mold are filled last and serve as risers to supply liqid material to the casting during recompression. After the mold is completely filled the vacuum is released. Resin in the vent/risers is drawn into any pockets that may have existed while under vacuum, the casting is cured in place.

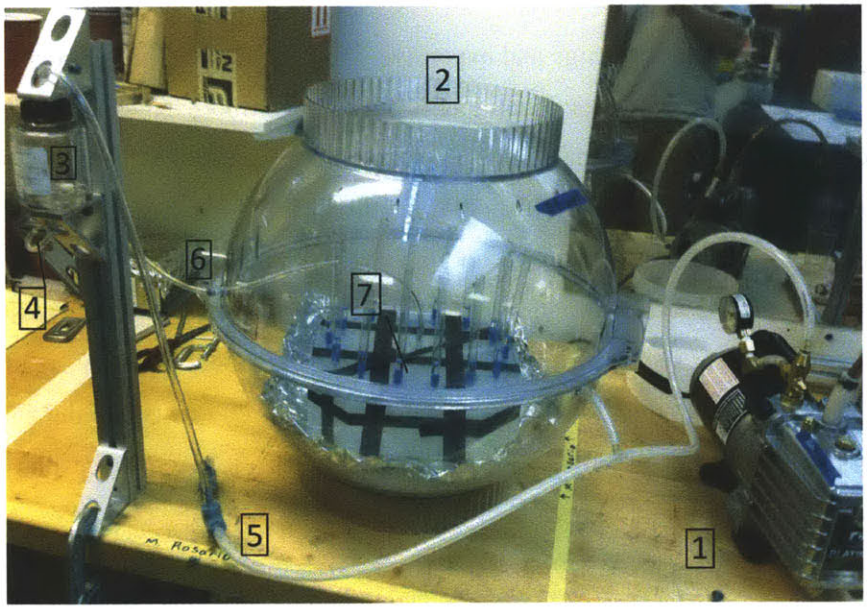

Figure 39

The chamber used is a polycarbonate dome that splits in the middle to allow easy access. The vacuum dome has two ports and it's transparency plays an important role in the casting process by allowing the user to monitor and control the mold filling. Polycarbonate is an ideal chamber material due to its toughness and clarity. The vacuum pump used is a 10CFM unit capable of 15μM of Mercury. The large throughput of the pump helps to quickly bring down the pressure of the chamber, a huge benefit when degassing mixed resin with short gel times.

3.2.5. Degassing the Casting Material

The Importance of degassing the casting material cannot be stressed enough. The best practice was found to be degassing the thermoset components individually, then gently and evenly mixing them to avoid the introduction of air, then degassing the mixed volume. Degassing is very important because if the material contains any dissolved gasses or bubbles it will foam vigorously as it enters the low pressure atmosphere inside the mold. A foam filled mold is nearly impossible to recover from and the casting is almost certainly ruined. A slow, laminar filling of the mold without bubbles is key.

Degas time for Epon 815c resin and Epikure3234 curative	Effect
none	Foaming as resin enters the mold, ruined casting
1min	Foaming and bubbles present, ruined casting
5min	No foaming, but noticeable expanding bubbles in resin supply line
15min	No foaming, no noticeable bubbles in resin supply line, smooth filling

3.2.6. Mold Filling Pressure

The mold filling pressure was also an important variable to a successful cast. One advantage to a higher differential pressure between mold and resin supply is faster filling especially with more viscous materials. However this advantage must be carefully balanced with the tendency of the casting material to foam under increasing vacuum due to volatiles evaporating. It was found that that the Epon 315c epoxy and curing agent contained volatile compounds that had a vapor pressure around 29.5inHg so that no matter how long the mix was degassed, if casting was attempted at or below 29.5inHg the mix would boil in the mold and make casting quite difficult. With the 315c epoxy mix best results were had casting at about 25inHg, this seemed to inhibit foaming and excessive bubble growth, while still providing vacuum casting advantages.

3.2.7. The Pinch Valve

In order to reduce material waste, provide greater flow control, and allow the unit to be automated for higher throughput and repeatability, a servo controlled double pinch valve was developed. The pinch valve is a flow control valve that is installed between the casting supply pot and the mold. One motivation behind developing this valve was to dramatically shorten the length of tubing between the casting supply pot and the mold. The advantages can be seen in the Poiseulle equation $\Delta P = \frac{L*128*\mu*Q}{\pi*D^4}$ where the pressure differential required to produce a given flow is linearly related to the length of the pipe (or tube in this case). The Servo valve allowed the tube length to be reduced from 16" to 7" resulting in a 56% reduction in differential pressure for a given flow, this could also be looked at as a ~130% increase in flow for a given pressure (all other variables held constant). This was not a huge factor for less viscous epoxies but is very important for more viscous materials where any amount of vacuum in the mold space is unable to draw material through the supply tube. Another motivation behind the servo valve is that it allowed the casting supply pot to be placed inside the vacuum chamber along with the mold; this negates the need for the casting supply line to run through ports in the chamber. These ports are ¼" ID and act as flow restrictions for more viscous or filled materials; the servo valve can accommodate up to ½" OD tubing. Reducing the amount of tubing that resin flows through greatly reduces waste in the process

because all tubing that the resin comes in contact with must be thrown away, and a good amount of resin is always left in the tubing after casting. Having the resin supply vessel in the chamber allows for materials with a very short gel time to be used because the degassing can take place while the mold is being pumped down, not in a separate process, this saves valuable minutes. Another motivation for the pinch valve is that it allows for the process to be fully automated in the future. Once parameters were established for a given mold and casting material. The process could be automatically repeated and reduce user involvement and increase process control and repeatability.

3.2.7.1. Servo Pinch Valve Design

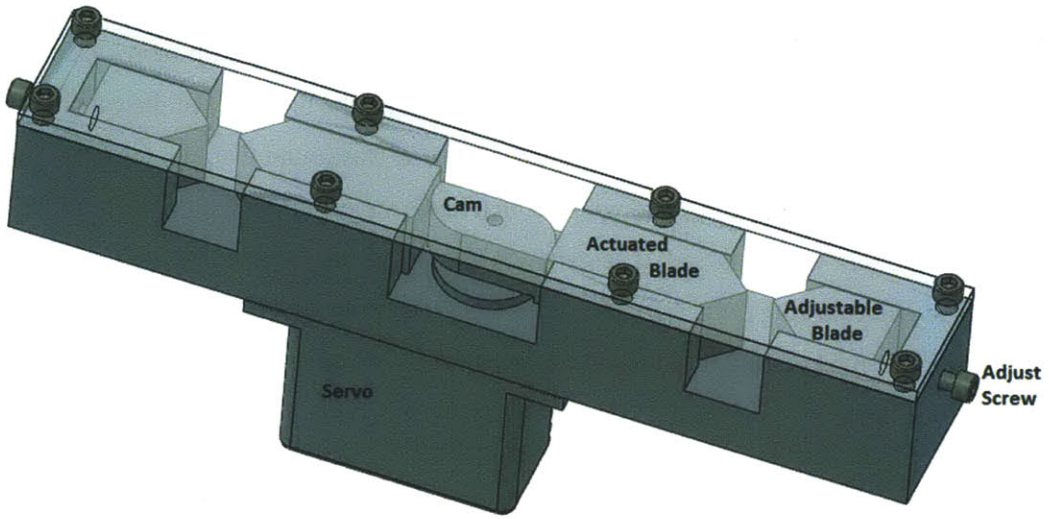

Figure 40
Pinch Valve model

The design requirements for the pinch valve are: 1) the valve can have no contact with the fluid 2) the valve must accommodate a range of tube sizes 3) the valve must provide variable flow control. A pinch style valve seemed ideal for this application since it avoids fluid contact. The design is based around a small hobby servo because they are cheap and provide high torque of 90in-oz. To convert the rotary motion of the servo to linear motion of the pinch valve, a cam and slider mechanism was developed. The cam and slider offer a number of distinct advantages: 1) The cam can be designed to provide a linear relationship between servo rotation and slider motion or a falling leverage ratio between the two so that the servo has more mechanical advantage as the tube is pinched. One could even design a feature in the cam so that zero holding torque is required when the tube is fully pinched off. The point here is that the cam provides many modes of operation and is easily changed to modify the function of the valve. 2) The sliders remove any tangential friction forces that the cam would experience if it acted directly on the

tubing and provide the proper geometric constraints for the cam analysis to be valid. To mitigate slider jamming a length to width ratio of 2 was used.

The valve is designed to pinch the tube in two places. This allows for more range in resistance adjustment since the fluid must pass through two resistances in series. More importantly the two tubes cause a symmetric load on both faces of the cam, this results is a pure torque on the servo and removes any bending moment on the servo shaft that would bind the motor and reduce the life of the valve. If necessary the valve can function in a single pinch mode. The backup sliders Figure 41 are adjustable to accommodate different tubing sizes.

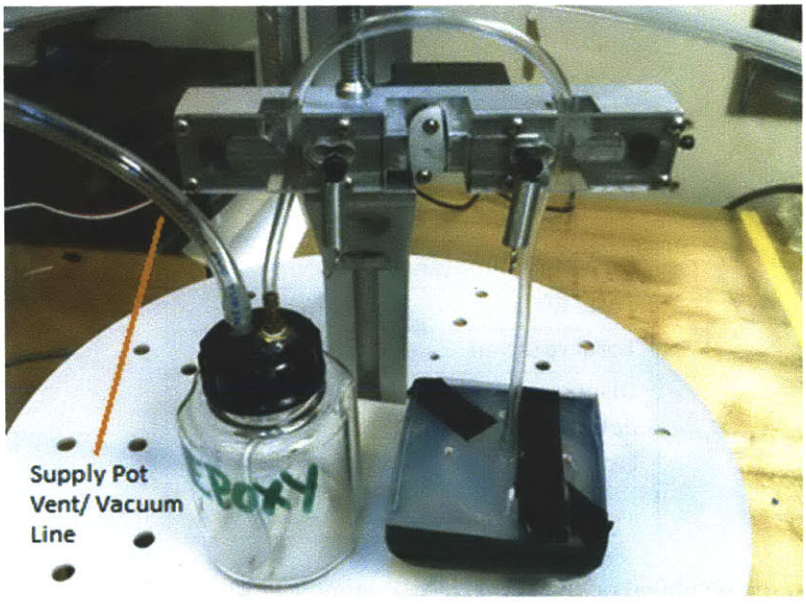

Figure 41

Figure 41 shows the pinch valve in operation with a small silicone mold. This is all inside the vacuum chamber.

3.2.7.2. Cam Design

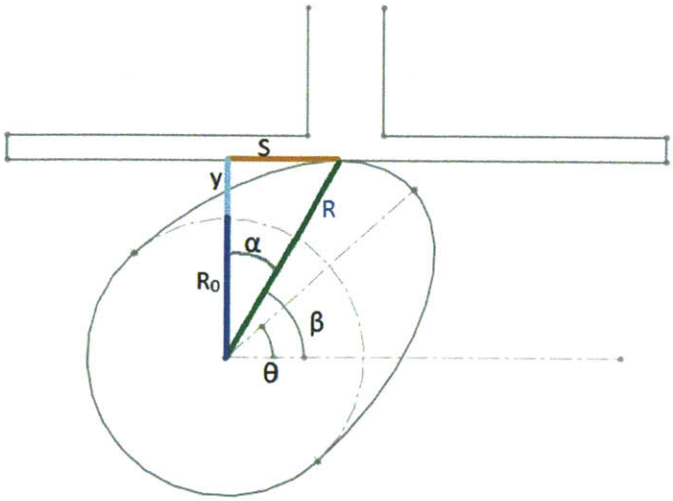

Figure 42

Design parameter	
Total lift	.3 inches
Total rotation	90 degrees
Displacement equation	R=k*θ (linear)
Lift constant k	.191

Table 3

To create the cam for the pinch valve, the radius of curvature R needs to be described as R=f(θ) in polar coordinates. Y, the lift height shown in Figure 42 is described by Y=kθ.

$$R(\theta) = \sqrt{(R_0 + y)^2 + s^2} \text{ where } y = k\theta$$

From Uicker (9):

$$s = \frac{dy}{d\theta} = k$$

Replacing : s and y

$$R(\theta) = \sqrt{(R_0 + k\theta)^2 + k^2}$$

Equation 1

This polar equation was used to create a cam profile of 180 points which was in turn converted to g-code and machined on an Easy-Track mill using DanCam. The cam profile output from Matlab is shown below in Figure 9 and the completed cam in the pinch valve assembly is shown in Figure 44.

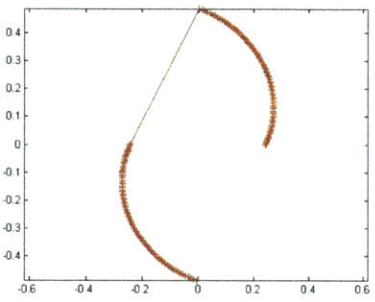

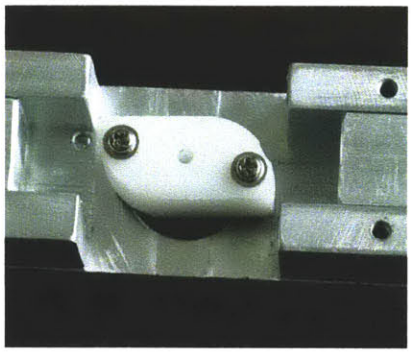

Figure 43

Figure 44

3.2.7.3. Lessons Learned / Improvements for Rev. 2

The main lesson from the pinch valve is the importance of designing for failure, a basic design concept that is not fully appreciated until the mistake is made. The servo actuates to pinch off the tubing, so the valve is nominally open. This is not what you want controlling the flow of casting material, this valve should be normally closed so in the event of failure the valve shuts off the flow. Lessons were also learned about designing slots for linear motion. In the interest of time and simplicity, the slots were all machined into the valve body. For low forces, speeds, and cycles, this was acceptable. However, careful attention must be paid to the depth of cut, cutter size, and milling technique when making this sort of slot to avoid irregularities in the sliding interface that may cause jamming. Figure 45 shows the importance of chamfering the slider to avoid interference due to imperfect cutter geometry.

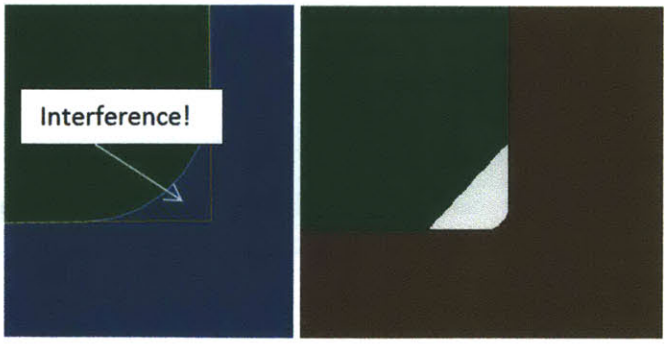

Figure 45

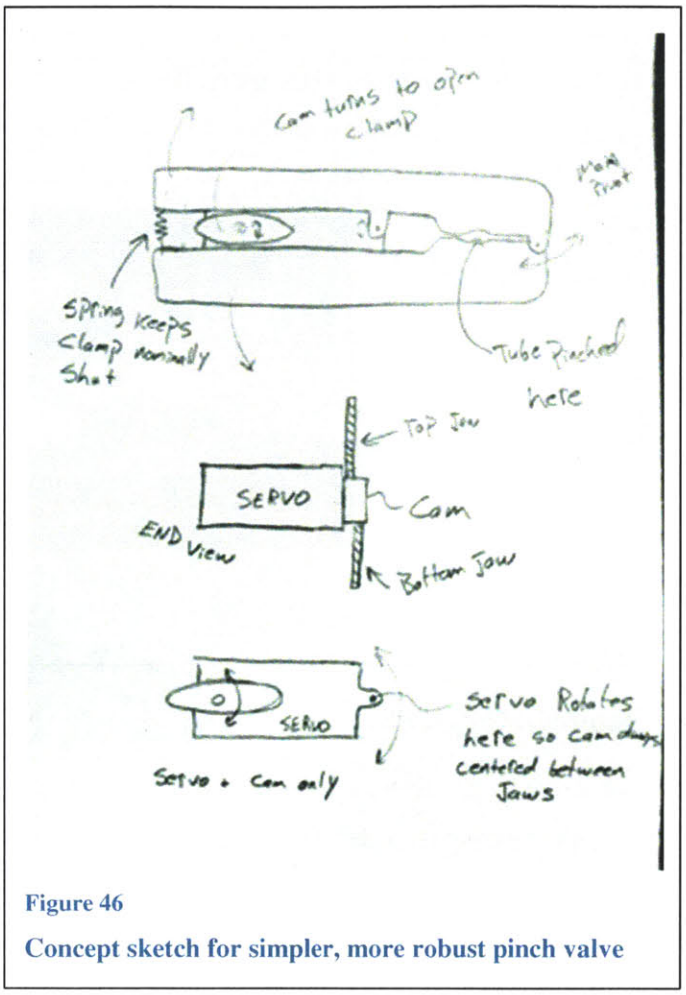

Figure 46

Concept sketch for simpler, more robust pinch valve

An improved design could be composed of two flat "jaws" hinged at one end and pinch the tube near the pivot, very similar to a nut-cracker. A spring at the opposite end would keep the valve nominally shut. A cam between the jaws would twist to spread them apart and allow fluid flow. The cam would be driven by a servo that pivots at one end to allow it to rotate in the flat plane of the jaws. This allows the cam to self-center between the jaws as they open and close. This design would be very easy to build, no bending moments would be applied to the servo shaft, and there is no concern about binding as the valve actuates.

3.2.8. Silicone Molds

Although vacuum casting can work with nearly any mold material, for this work silicone molds were selected due to their ease of manufacture and excellent release properties. Typically when working with thermosetting resins (or almost any casting and molding operation), careful attention must be paid to the surface finish of the mold and a variety of surface treatments must be applied to prevent the part from being stuck into the mold. Silicone adheres very poorly with the casting materials used (epoxies and polyurethanes), no special surface preparation was needed. Typically a mold is cast off a master model,

this master model must have excellent surface finish which requires extensive smoothing and polishing. With the silicone molds, master models could be used immediately after machining or 3d printing to cast the molds with little to no attention paid to their surface finish. Attempting this with any other cast-able mold material would result in your master model being permanently adhered in the mold. Another advantage to the silicone molds is their flexibility. Having a flexible mold allows features like small undercuts to be cast without needing much more complicated multi-piece molds. Having a flexible mold makes demolding quite easy compared to the often frustrating and lengthy process of removing parts from hard molds. Silicone molds allow can produce complex parts with features like undercuts and are often used to create functional prototypes for parts that are to be injection molded.

The expected mold life is around 50 parts and sometimes up to 100 depending on the mold geometry and the use silicone sprays to keep a fresh mold surface.

Table 4 below shows a comparison of cost between some common casting materials.

Material	Cost
Freeman 3040 clear silicone	40 $/Liter
Freeman 340 opaque silicone	46 $/Liter
urethane	34 $/Liter
Plaster	2 (at 70cc mix ratio) $/Liter

Table 4

The flexibility of Silicone molds is a great benefit during demolding, but during casting it can be a challenge. During mold filling the flow rate must be kept quite low to avoid pressure from building up in the mold due to flow resistance of the casting material. Initial tests confirmed that filling the mold too quickly caused the mold to bulge and the seal around the parting line to fail resulting in epoxy resin leaking out. For thin walled castings, flow rates of 1mL/s worked well based off knowing the casting volume and time to fill.

Mold closure force is an important parameter is setting up for vacuum casting. This closure force is:

$$F = A_{projected} * P$$

P is the differential pressure between the resin supply and mold, and A is the area of the casting projected onto the parting plane. Rigid backing plates or tape wrapping was needed to prevent the mold halves from separating during filling.

To get a simple closed form solution for approximating how thick the mold needs to be, the mold can be approximated as a simply supported rectangular beam with a distributed pressure load. This is a worst case approximation because the mold section is assumed to be supported on only two ends, not all 4 sides

like a membrane. The equation for the maximum deflection of a beam is: $v_{max} = 0.156\frac{pl^4}{Eh^3}$ where v is the deflection, p is the internal mold pressure, l is the effective mold length, E is Young's modulus, and h is the thickness of the mold section. Solving for a ratio where v_{ok} is the acceptable deformation :

$$\frac{h}{l} = .54\left(\frac{pl}{Ev_{ok}}\right)^{1/3}$$

Equation 2

Since the mold is made of an elastomer, a relationship must be used to convert from shore hardness to Young's modulus. From Qi (10) $\ln(E) = .0235S - .6403$ where E is the modulus in MPa and S is shore A hardness for materials with an $20<S_A<80$. Using this relationship we can approximate the modulus of the 3040 molding silicone to be about 1.29Mpa. Inserting this value into Equation 2 with a v_{ok} of 4mm, a pressure of 1psi (7.14e3 Pa), and an l of 12" (.3M) we get a thickness to span ratio of .4 or a minimum mold thickness of about 4.8" inches for a span of 12." This deformation approximation highlights the major problem with using silicone molds, the low stiffness of the molds severely limits fill pressures and necessitates some sort of rigid support.

3.2.9. Making the Silicone Molds

Creation of the silicone molds for casting involves six major components: 1) the master model 2) the mold box 3) master mounting and sprue placement 4) the vents 5) the parting line 6) the silicone itself.

1) Master model

The master model is the first step in making the silicone molds. The big advantage to this process is that the master model can come from just about anywhere. It can be 3d printed with FDM, SLA, or inkjet methods. It can be an existing item, made of wood, machined, cast, etc. Careful attention must be paid to how the master and part will be removed from the mold. Silicone molds can handle minor undercuts and no to negative draft. Careful attention must also be paid to how the mold will be filled and vented as this will determine the orientation of the master model for pouring the mold. Porous surfaces such as wood should be sealed with something like Freeman's wood sealer, otherwise almost any surface will suffice as long as a light spray of petroleum jelly mold release is applied.

2) Mold box

The second element, the mold box, is usually constructed of wood or melamine board. The box should allow for the minimum thickness of 1 inch around the part and an h/l ratio given in Equation 2. The box should be sealed so liquid silicone doesn't leak out and easily disassembled for easy removal of the cured

silicone mold. It is important to make the mold box at least twice as high as the free surface of the silicone for degassing purposes.

3) Sprue

The third component is the master model mount and sprue location. For the work presented here a 3/8 wooden dowel was fixed to the master model which served as a post for suspending the master model in the center of the mold box. This dowel also formed a sprue after being removed. In this work only one sprue was used and extended to the lowest portion of the mold.

4) Risers

The fourth component of mold construction is the risers. Risers must be placed at all the high spots in the mold and are last to fill. Risers also provide places for errant bubbles to escape during filling. Risers should be placed so that the flashing left behind can be easily removed and does not interfere with the part function. In casting the brain holders, risers were placed along the outer edge of the sealing flange, not on the sealing face as the process to remove flash could damage the sealing face. It is also advantageous to make critical surfaces face down since bubbles collect on upward facing surfaces. To construct the risers ¼ dowels or rods were hot glued to the master model and extended out of the silicone. It's important that these easily break away from the master model so that after the silicone is cured the master model can be easily removed and the vent dowels or rods can be easily removed.

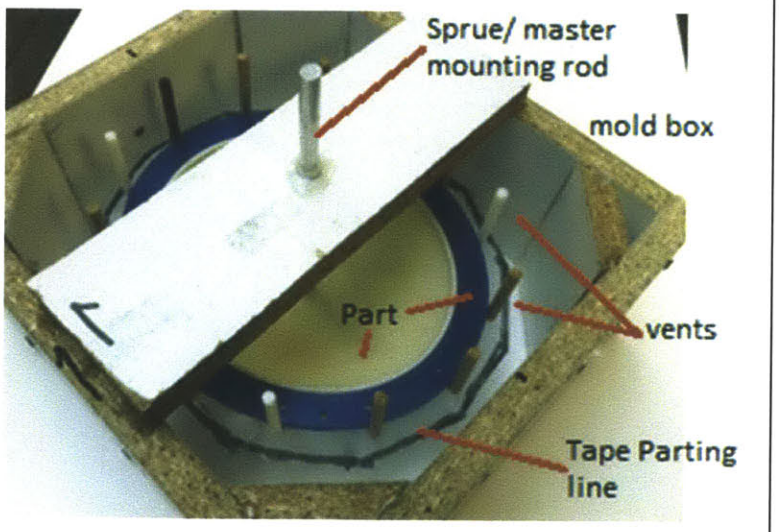

Figure 47

5) Parting line

The fifth component is the parting line. A very useful technique is to use scotch tape to create a thin parting surface, extending out from the parting line, and to color the outer edge of the tape with a marker. When slicing the mold open the marker line is visible through the silicone and creates a reference to cut up to for splitting the mold. Care must be taken to keep the parting surface very thin. 1 layer thick of scotch tape works well, three layers were tried and the parting surface was to thick and caused the mold to leak.

6) The silicone

The sixth and final component is the silicone itself. Freeman's v-3040 silicone was used; it has a 39A shore hardness, 120 pounds/in. tear strength, 1 hour pot life, and is translucent. A translucent mold was critical for the mold making technique employed where the whole mold is poured in one shot and the parting line cut after curing. Degasing the silicone after mixing is absolutely necessary due to the air introduced during the mixing process. A container at least twice the volume of the silicone must be used due to the extreme foaming during degasing. Finally the degased silicone must be slowly poured down the side of the mold box to avoid air entrapment.

After the mold is cured a scalpel and spreading pliers are used to cut down to the edge of the tape parting plane (colored so it can be seen). Once the mold is cut all the way around and down to the outer edge of the tape the mold can be split and the master removed. The mold is ready for casting.

3.2.10. Casting Process and Results

Appendix B outlines a basic vacuum casting procedure. The following troubleshooting guidelines may prove helpful for future work.

Problem	Cause	Fix
Resin leaks out sides of mold	Filling to fast	Slow filling, lower pressure differential, use electrical tape to seal mold
Air pockets around vents + resin overflowed vent during casting	Vents are too small, need risers	create external risers to hold extra casting material that will flow back in when vacuum is released
Foaming of casting material or bubbles observed in feed line	Air trapped in casting media	Degas more thoroughly, transferring degased resin to another vessel can introduce air
Very slow or no flow of casting material	material is gelling/curing, pinched feed line	Mind your pot life, do not overmix, use semi-rigid tubing
After mold removed from chamber excessive resin flows out of riser or feed line	Liquid material is reaching hydrostatic equilibrium	Think of your mold and vent lines as being filled with water that you don't want to spill. The liquid material will try and reach the same height in the feed line ad risers, this may cause air to get sucked in under certain circumstances

Table 5

Figure 48

detail shot showing reproduction of tiny serial number

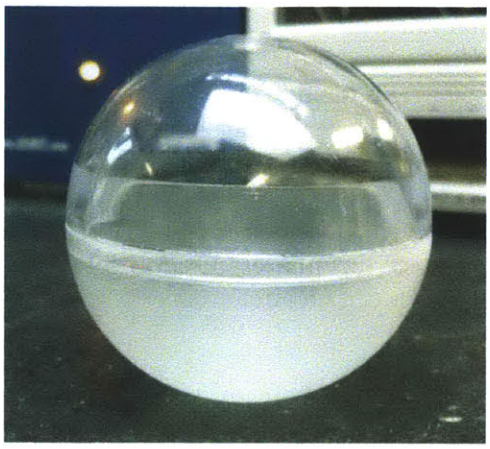

Figure 49

cast copy snaps with original opposing half

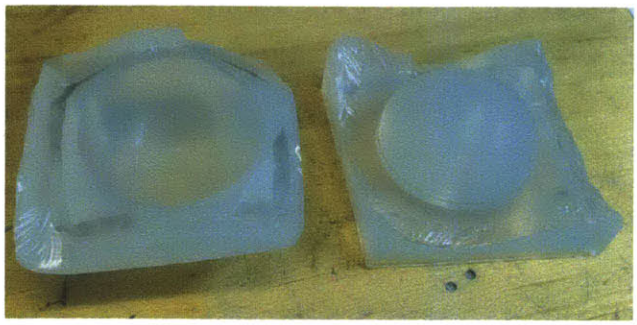

Figure 50

Small test mold split

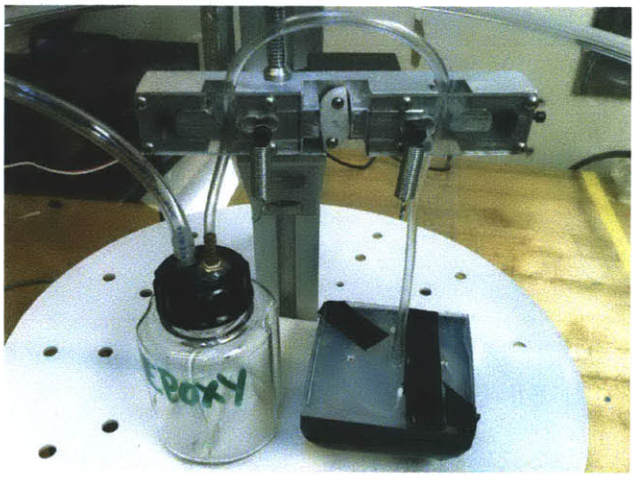

Figure 51

test mold during casting

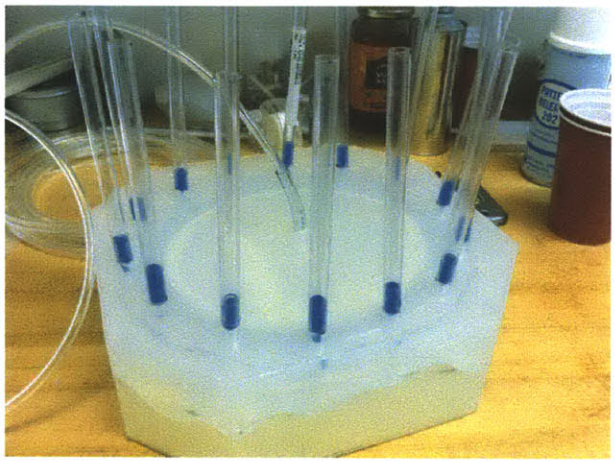

Figure 52

Top brain holder mold ready for casting

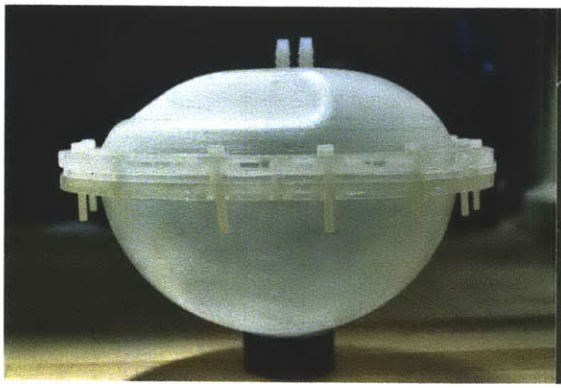

Figure 53

Finished castings assembled

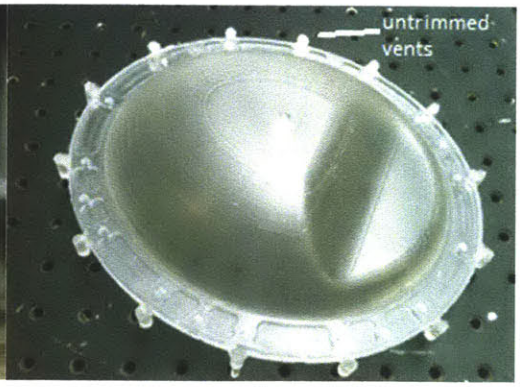

Figure 54

Finished part after demolding

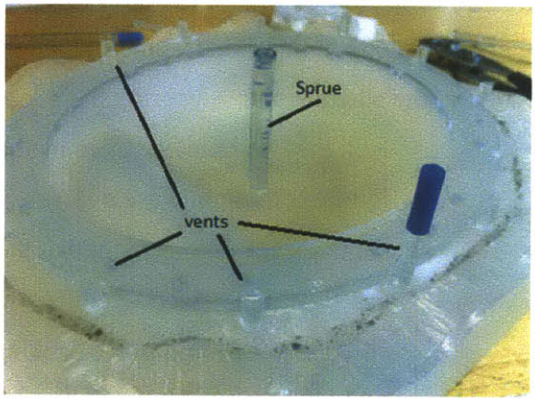

Figure 55

Finished part still in bottom part of mold

3.2.11. Hybrid Molds

Full silicone molds have a major disadvantage, their low stiffness means they can handle very little internal pressure. To address this some experimentation with a hybrid hard/soft mold was done. The idea was to combine the excellent release properties of the silicone with a stiff, less expensive bulk material. In this test a thin (1/4") layer of silicone formed the mold surface and behind that, providing support, would be a thick body of plaster. The mold had to be made one half at a time with a traditional hard parting surface, but was still relatively easy to make. Thin layers of silicone were brushed over the surface of the master until the desired thickness built up, and after it cured, the mold box was filled with plaster.

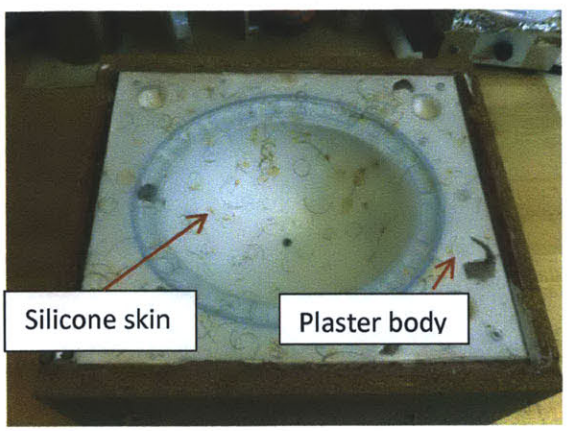

Figure 56

The problem encountered was that the silicone mold "skin" would not adhere or stay put in the plaster. Chopped steel fibers were imbedded in the silicone before pouring the plaster in an effort to mechanically lock the two together. The method worked reasonably well. Future tests should use a larger quantity of fibers or perhaps some sort of porous foam that the both the silicone and plaster can flow into. Another concept would be to simply allow the silicone to be loose in the backing. This would work if the mold had a positive pressure to push the silicone up against the plaster. It could also allow for more extreme undercuts and similar feature to be molded because the silicone could be used to fill the undercuts on the part side while providing an even, easy-release surface for the plaster on the other side. Upon demolding the part with the silicone skin would slide out of the plaster mold and the mold skin "peeled" off. Because it is so thin the skin would be very flexible for demolding.

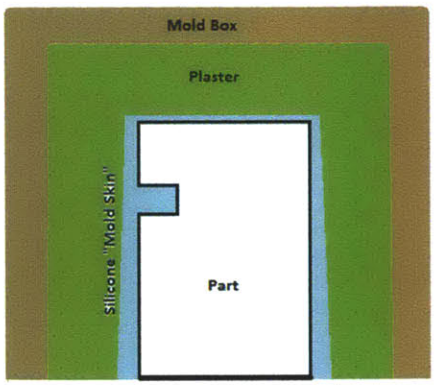

Figure 57

Hard molds were also used in this work. The molds were machined from polycarbonate plate and used to vacuum cast silicone gaskets for the brain holder. The shape of the gasket was machined into one plate using DanCam (section 3.3) than a face plate was bolted down to seal the mold. Here only one vent was used, so the mold had to be filled slowly to avoid the vent being blocked of by material before the filling was complete.

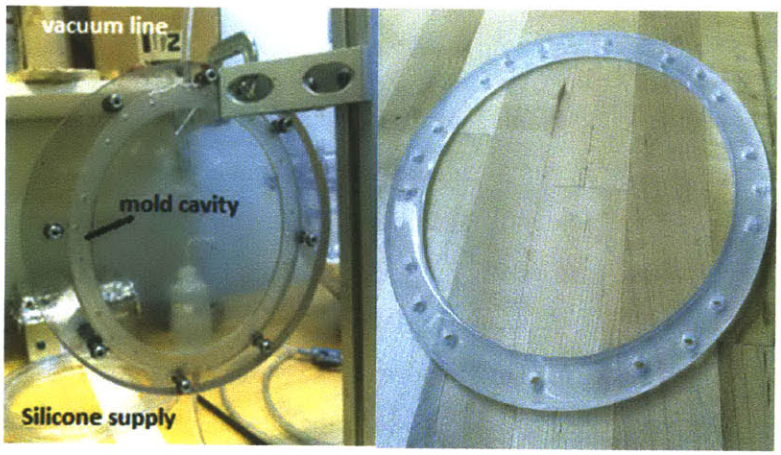

Figure 58

3.2.12. Flow Analysis

Before casting some analysis needed to be done to insure that the casting pressure differential of ~14psi would be enough to drive the Epon815c casting epoxy through the feed lines. To begin it was assumed that the flow would be laminar and that Poiseulle's equation applied. Solving for flow rate Q :

$$Q = \frac{\pi D^4 \Delta p}{128 \mu l}$$

D	.0034 M
Δp	94458 N/M2
μ	.7 Ns/M2
l	.3 M

Q=1.47e-6 M^3/s

This flow rate is then used to go back and check the laminar assumption:

$$Re = \frac{\gamma v D}{\mu}$$

D	.0034 M
v	.162 M/s
μ	.7 Ns/M2
γ	1127Kg/M3

Re = .89 ← very laminar

3.3. DanCam

3.3.1. Motivation

Conventional CAM (Computer Aided Manufacturing) programs such as GibbsCam, MasterCam, SolidCam, and many others, are large, complicated, and very capable programs. Packages usually start at a few thousand dollars per seat for basic mill capabilities. Due to the skill and cost constraints many small shops and labs cannot afford to use these programs. Additionally many designs do not require advanced surface milling capabilities. Many designs are best reduced to 2 or 2.5 dimensional machining. As part of this thesis DanCam was written in Matlab to be a very easy way to automatically generate toolpaths from .stl files. All the user needs to do is select the tool diameter and the cutting plane heights then the program will generate the profile and pocket paths. STL files are ubiquitous now thanks to 3d printing so geometry can be created in any CAD program. DanCam was born out of the frustration of using one of the large, very popular CAM software packages which shall remain unnamed. The largest frustration was having to redo much of the toolpath when even the smallest design changes were made. This wasted valuable time; the CAM program proved to be unwieldy, unintuitive, and required user input for every machining feature and step. The idea of DanCam is that small shops or labs can use a low cost numerically controlled mill such as an EasyTrack or retrofit a manual knee mill with NC controls (both options are relatively low cost and widely available) and easily program these machines with DanCam to rapidly and cheaply create prototype parts.

3.3.2. The .stl File

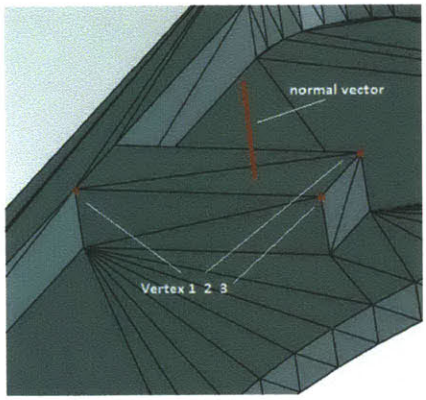

Figure 59

.stl files are a way of representing the surface geometry of a 3d object. The surface of the object is tessellated into triangles and the .stl file lists the coordinates for the three vertexes and a unit normal vector. Figure 59 shows a visual representation of a rendered .stl file. STL's have a binary and ASCII format, DanCam uses the ASCII format.

DanCam completes 6 major steps: 1) Importing the .stl file and preparing the data for processing 2) finding facet intersections with the z slice plane 3) sorting the intersection line segments 4) forming the path and tool offsets 5) pocket path creation 6) writing to G-code.

3.3.3. Importing the .stl

The created function "extract_lines2.m" reads the ASCII file in line by line placing the facet coordinates and the normal vector into a facet array. Each array is sorted in descending order according to the z coordinate of each point. Then all the facet arrays are put in order according to their lowest (in z) vertex. This data is saved out in a .mat file for subsequent use.

3.3.4. Finding the plane-line intersects

The function "extractall.m" takes the sorted .stl facet data and starts looking for facets that intersect an XY plane at a predetermined Z height, this is called the slice plane. This is where sorting each facet array comes in handy, the program looks at each facet array and decides if its lowest vertex is below the selected slice plane. If so then the program will look to see if either or both of the other vertices are above the slice plane. If so then we have a line formed in the slice plane where the facet and slice plane intersect. This line is a piece of a cross section of the part in the slice plane.

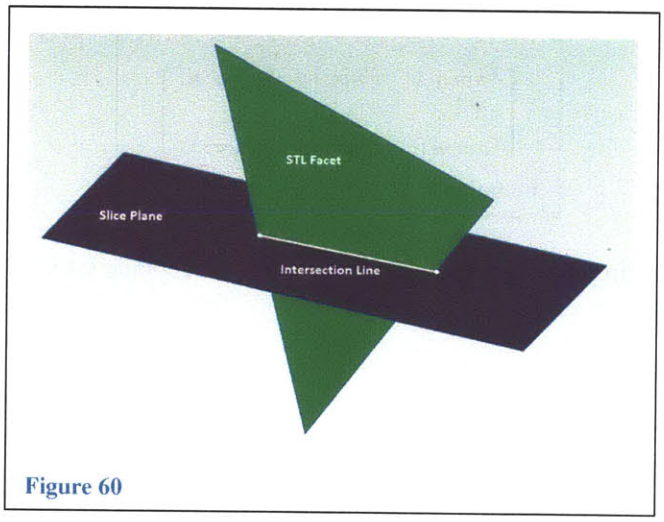

Figure 60

The line segment is found by first finding the *points* of intersection between the edges of the facet that intersect the slice plane using the created function "plane_line_intersect(n,V0,P0,P1)" (n: normal vector of the Plane, V0: any point that belongs to the Plane, P0: end point 1 of the segment P0P1, P1: end point 2 of the segment P0P1). Now these two points simply form the line segment at the intersection of the slice plane and the facet.

The result of this line finding process is an array of jumbled line segments. The segments must be linked together so that they form a continuous path. The algorithm randomly picks a starting segment, with this it searches the other remaining segments for a point that matches one of its points. This matching point becomes the "tail' of the first segment and the "tip" of the second segment. The algorithm repeats this matching process for the second segment and through all the segments chaining together the perimeter.

Since most parts have more than one continuous face (think cylinder vs tube) there will be multiple perimeters or "loops" as they are called in the program. When the program has strung together n segments and ends up back where it's started that loop is complete and is saved, if there are still unsorted line segments left the process starts on those saving each ordered loop in an array until all the segments are used up. The segments are saved in their own loop array as:

$$\begin{bmatrix} tip1 & tail1 \\ tail1 & tail2 \\ \vdots & \vdots \\ tail\ n & tip\ 1 \end{bmatrix}$$

Equation 3

And the corresponding normal vector components for each line segment are stored as:

$$\begin{bmatrix} x_{norm1} & y_{norm1} & z_{norm1} \\ \vdots & \vdots & \vdots \\ x_{norm,n} & y_{norm,n} & z_{norm,n} \end{bmatrix}$$

Equation 4

The "pseudo-code" for forming line segments from the faces / sliceplane intersection is shown below.

```
For all facets k=1:n
        If facet(k) lowest point < slice plane height
                facet(k) low point = point 1
                Other facet(k) points = point 2 and point 3
                if point 2 & point 3 > slice height
                        I1=plane_line_intersect(point1,point2)
                        I2=plane_line_intersect(point1,point3)
                        Segment(step)=line(I1,I2)
                        Normal(step)=norm(k)
                        Step=step+1
                elseif point 2 > slice height &  point 3 <slice height
                        I1=plane_line_intersect(point1,point2)
                        I2=plane_line_intersect(point3,point2)
                        Segment(step)=line(I1,I2)
                        Normal(step)=norm(k)
                        Step=step+1
                elseif point 2 < slice height &  point 3 >slice height
                        I1=plane_line_intersect(point1,point3)
                        I2=plane_line_intersect(point2,point3)
                        Segment(step)=line(I1,I2)
                        Normal(step)=norm(k)
                        Step=step+1
                end
        end
end
```

3.3.5. Tool Offset

To create the tool offset, DanCam creates an offset line segment for each original segment in each loop. It does this by using the normal vector data stored with each segment. The normal vector is projected onto the XY slice plane then creates a new line by moving the segments endpoints a specified offset distance in the direction of the projected normal vector. However this leaves offset line segments with endpoints that do not match. To solve this the program takes the newly created offset line and the offset line before it and uses "my_intersect.m" to solve for the intersection of these lines, this becomes a point in the new offset tool path. This is shown schematically in Figure 61. Using Matlab's "subspace" function, the angle between offset lines is evaluated. If the angle between the lines is under a threshold of some user set value, then the intersection of the offset lines is not added to the tool path and the program looks

for the next new point to add. This is an excellent feature for reducing the size of the G-code because a .stl file will often have tessellations all across a flat surface. The G-code for the path along this straight surface need not include many intermediate points, all it needs is a point at the beginning of the straight path and the end. This filtering feature reduces the quantity of G-code considerably.

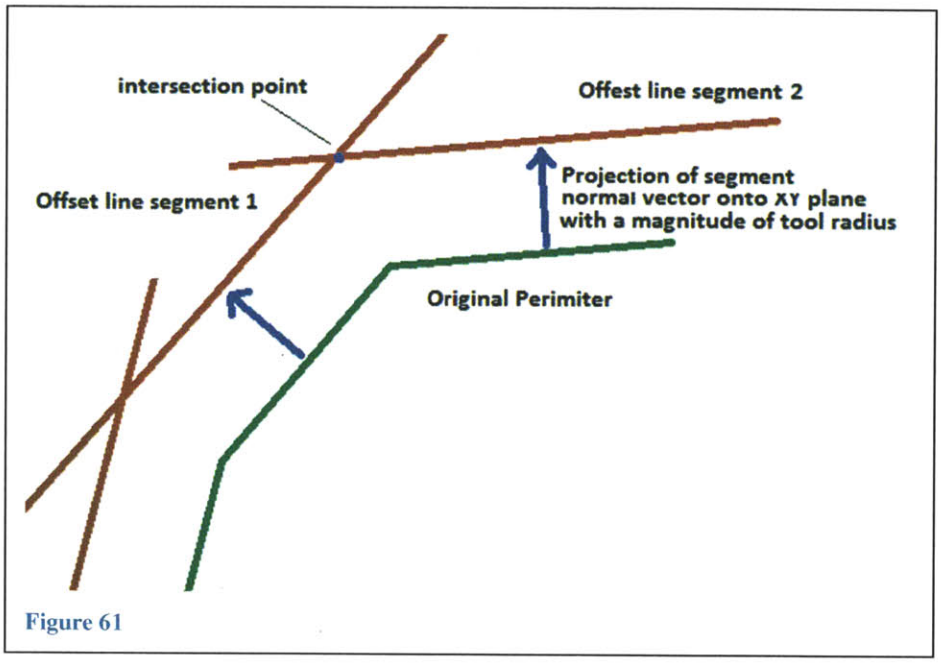

Figure 61

The program "pocket.m" creates g-code for pockets. It is a basic zigzag style pocket for program simplicity that can be executed before or after the pocket perimeter is cut. It works by creating evenly spaced "step over" lines running in the X direction, it then searches to find where the tool path intersects these lines. When doing the zigzag pocket the tool will run along these lines from intersection point to intersection point. The program knows whether to plunge or retract at each intersection depending on whether the intersection is an odd or even number in its sequence along the stepover line. Figure 62 shows this pictorially. Since the pocket uses the *offset* tool path as a reference, it can plunge *at* the intersection of toolpath and step over line without worry of plunging into the wrong section of the part

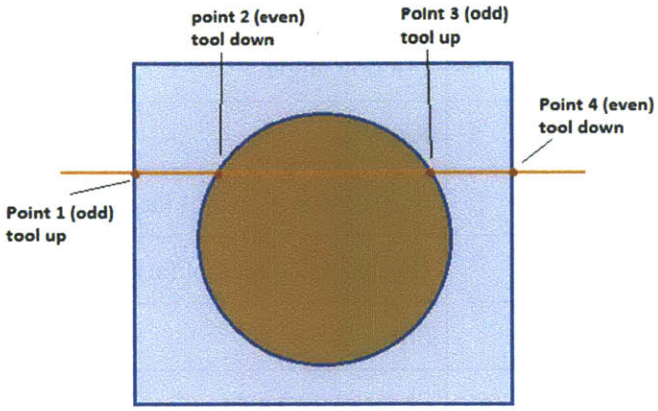

Figure 62

The final offset toolpath is finally written to G-code and saved in a text file ready to be exported to a machining center. Parameters such as spindle speed, feed rate, retract plane, slow z plane, tool diameter, and pocketing options are set at the beginning of the "tool_path.m" file. Below are a few pictures of DanCam in use; Figure 63 and Figure 64 show machining in wax and Figure 65 shows a pair of polycarbonate parts.

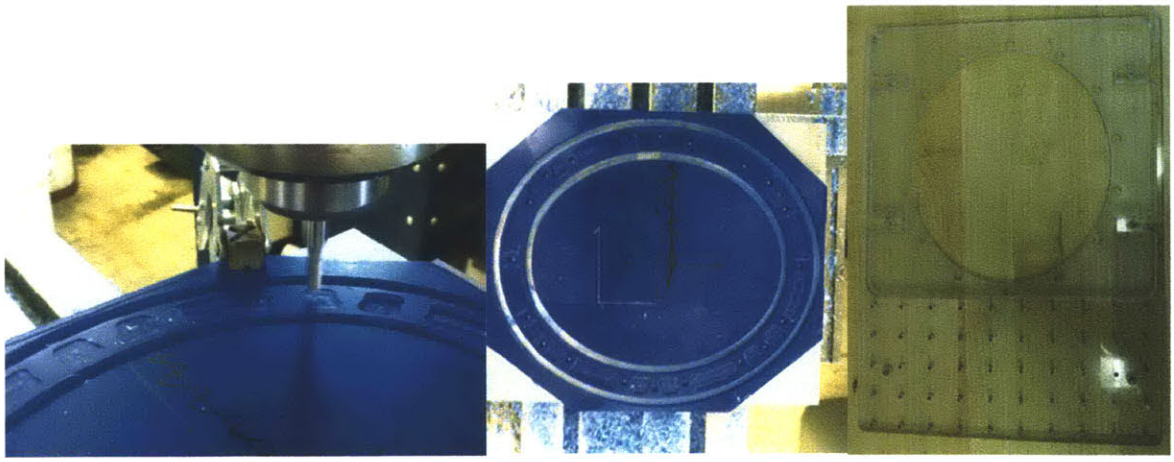

Figure 63

Figure 64

3.4. Calculating Cutting forces and machine requirements

To make appropriate selections of machining parameters and part fixturing, estimates of cutting forces and machine power were required. Figure 66 shows a simple force balance on the tool and chip based on the M.E. Merchant model. Parameters are summarized below in Table 6.

Variable	Quantity
α	Rake angle
β	Friction angle
R	Resultant force
F	Friction force on tool face
N	Normal force on tool face
Fs	Shear Force
Φ	Shear plane angle
Fc	Cutting force
FT	Thrust force
b	In plane depth of cut
h	Cut depth
Ls	Length of shear plane in shear direction
τ_s	Ultimate shear strength

Table 6

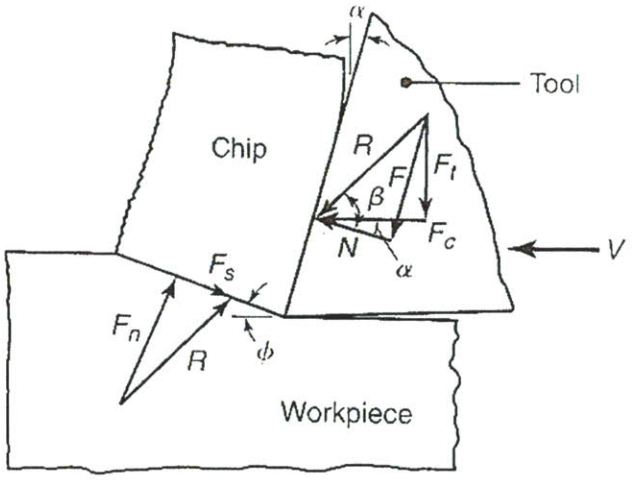

Figure 66 (9)

$$F = \sin(\beta)R \quad and \quad N = \cos(\beta)R \quad (1)$$

From Coulomb friction: $F = \mu N$ combining this with (1):

$$\beta = \tan^{-1}(\mu) \quad (2)$$

Next note that: $F_C = \cos(\beta - \alpha)R$ (3) $where$ $R = \frac{F_S}{\cos(\beta-\alpha+\varphi)}$

However F_s is unknown but can be found by stating $F_S = A_S \times \tau_S$

Where A_S is the shear area and τ_S is the ultimate shear strength, thus:

$$F_S = L_S b \tau_s \quad (4)$$

Rewriting (3) in terms of cut depth and shear angle:

$$F_S = \frac{h}{\sin(\varphi)} b \tau_s \quad (5)$$

Finally (5) back into (3)

$$F_C = \frac{hb\tau_s \cos(\beta-\alpha)}{\sin(\varphi)}$$

Equation 5

Where from the Merchant cutting model (11) :

$$\varphi = \frac{\pi}{4} + \frac{\alpha}{2} - \frac{\beta}{2} \text{ where from (2) } \beta = \tan^{-1}(\mu)$$

Equation 5 was used to determine the suitability of fixturing options for machining the large flat polycarbonate plates in Figure 65. The challenge in these parts was the need machining large pockets and all the way around the perimeter. The aspect ratio of the part precluded the use of a vice, the perimeter machining made toe clamps difficult, the best option was to use double stick tape to adhere the stock to a fixture base plate. Equation 5 allowed this arrangement to be analyzed and ok'd before going to the machine, this is summarized below in Table 7.

Parameter	Value
α Rake	10°
b depth of cut	.2 inches
h chip load per flute	.007 inches
Ts Tensile strength in Psi	9180 Psi (12)
μ coefficient of friction	.35
Calculated cutting force	30 Lb

Table 7

The 3M tape used had a shear strength of 110 Psi, and the taped area was approximately 40 in^2 so the 30lbs cutting force was well under the strength limit of the tape bond. The quantity of taped area and the thinness of the tape provided the required stiffness for machining.

4. Manufacturing The 32 Channel Ex-vivo Scanning Assembly

The inseparable relationship between design and manufacturing methods is expressed in this work by how design drove manufacturing methods where possible, but often the design was shaped by the manufacturing methods available.

4.1. Inner Brain Holder

Vacuum casting was selected to make the holders because of the need for multiple identical copies, low cost, and choice of materials. The shell portion of the master model was 3d printed and the sealing flange was machined to ensure good surface finish and flatness. From this master model a silicone mold was cast and that mold used in the vacuum casting process to produce the finished holders. Two small ports were epoxied in after casting to accomidate the degas process. Some changes in material selection were made due to the brittleness of the Epon815c cast epoxy. Due to the brittleness of the cast epoxy holders, new sets of holders were cast in rigid polyurethane whose properties are summarized in table 1. These holders proved to be much more resilient and able to withstand small inadvertent drops and rough handling. Figure 53 shows the finished cast holder pieces assembled.

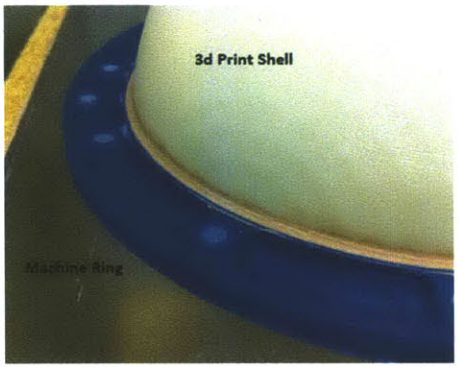

4.2. Receiving coil former

The receiving coil formers were made on a Dimension 3d printer. 3d printing was an ideal process for the formers because of the many complex features like the coil layout hexagons and amplifier mounting bosses.

4.3. Mounting Plate

The mounting plate serves as the interface between the bucket/ former, electronics mounting, and birdcage. This part was machined from ½ polycarbonate sheet because it's easy to machine and very tough. All CNC programming was done in DanCam and the part was machined on an EzTrak knee mill. Two iterations of the plate can be seen in Figure 65.

4.4. The Bird Cage

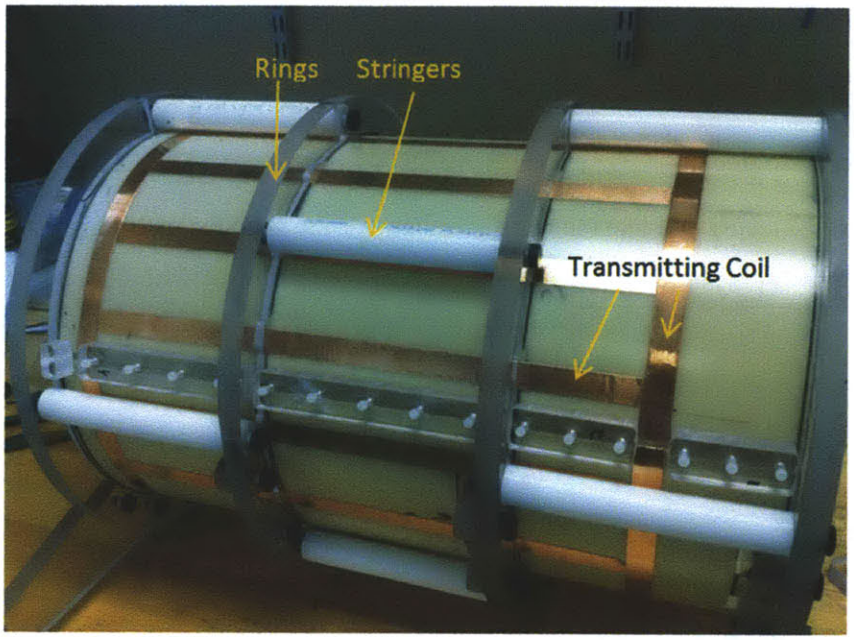

Figure 67

The initial transmitting tube was .04" polycarbonate which was selected for its high toughness. However, when subjected to repeated soldering in the same location, the material cracked due to thermal fatigue. A revised design incorporated a FR4 fiberglass/ epoxy sheet 0.031" thick because of its high strength, crack resistance, and high temperature resistance. Additionally the FR4 sheet had been used successfully in previous designs. FR4 has a CTE roughly $1/7^{th}$ of polycarbonate's and a thermal conductivity 44% greater making it less susceptible to thermal fatigue. The seam clamps shown in Figure 68 were critical to making the FR4 design work.

These seam clamps enforced a tangency constraint on the opposing edges of the rolled sheet forcing it to take on a round instead of teardrop shape. The nominal residual stress in the G10 sheet due to rolling is calculated in Equation 6 and is found to be roughly 12% of the ultimate flexural strength, allowing for a generous overhead for thermal stress induced by soldering.

Property	Value
Flexural Modulus	2700ksi
Flexural Strength	65ksi

Table 8 (19)

$$\epsilon_{max}=\frac{t}{2\gamma}=\frac{.031in}{2*5.1in}=3e-3$$

$$\sigma_{max} = E\varepsilon = 2700ksi * 3e - 3 = 8.1ksi$$

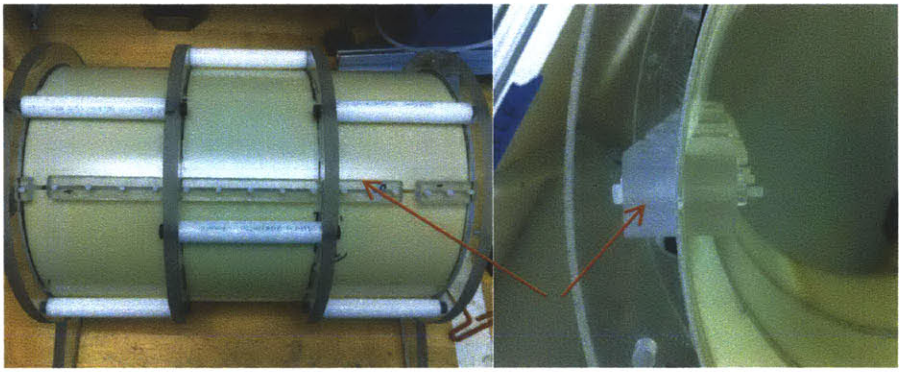

Figure 68

The skeleton of the birdcage is based on a "ring and stringer" design discussed in 2.7.2. The evenly spaced frame rings provide structure for the transmit coil former (the inner tube), while the stringers (white bars) align and evenly space the rings. The stringers were faced on a lathe to insure tight flatness and length tolerances. After assembling the skeleton, the copper coils are bonded onto the flat former sheet which is the rolled and inserted into the frame. The mounting plate brackets connect face to face with the rings taking advantage of the flatness of the stock surfaces.

4.5. Reducing thermal stress during soldering

ϵ_f	Strain of fiber in final state
ϵ_b	Strain of fiber due to additional bending only
ϵ_h	Strain of fiber due to heat gradient only
σ	Final stress
σ_b	Stress from bending to final state without any heat
σ_r	Stress relieved by thermal gradient
α	Sheet coefficient of thermal expansion
ΔT	Temperature differential across sheet
y	Distance from neutral axis to fiber
y_h	Distance from the bottom of the sheet to some fiber
t_0	Thickness of sheet
E	Modulus of elasticity
ρ_h	Free curvature from thermal gradient in sheet
ρ_f	Final imposed curvature of sheet

Table 9

After the polycarbonate sheet cracked due to thermal cycling, heat sinks were explored to reduce thermal stress in the birdcage former sheet during soldering. Heat induced sheet cracking so can reciprocity be applied to actually use this heat to reduce stress during soldering? The idea of the heat sink design is to use the pre-existing tensile stress (from forced curvature) in the upper fibers of the sheet to mitigate stress from thermal expansion. A heat sink is to be placed directly under the soldering area thus creating an approximately linear thermal gradient through the thickness of the sheet. The strain from this gradient due to thermal expansion is shown in Figure 69 as well as the strain and stress from the forced curvature without any heat applied.

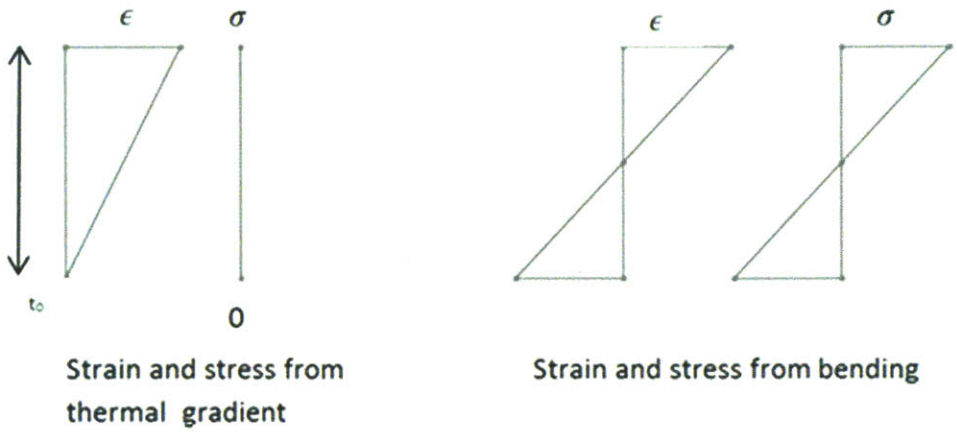

Figure 69

To analyze the change in stress of the rolled former skin, the strains and stresses from heating and bending are examined separately. According to the principle of superposition the final stress state is a sum of contributions from each process. First consider the strain and stress from heating only. In steady state there exists a linear thermal gradient through the thickness of the material ΔT. Due to thermal expansion the strain through the thickness is:

$$\epsilon_t = \alpha \Delta T \frac{y_h}{t_0}$$

Where y is distance up through the sheet and t_0 is the sheet total thickness. The strain is maximum on the outer surface and zero on the inner surface.

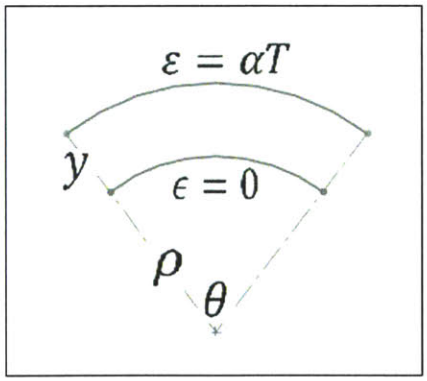

Solving for the chord lengths of the inner and outer fibers:

$$\theta\rho = l$$

and

$$\theta(\rho + t_0) = l(1 + \alpha\Delta T)$$

Solving for $\rho_h = \frac{t_0}{\alpha \Delta T}$

ρ_h is the curvature radius that the sheet would naturally assume in a free state.

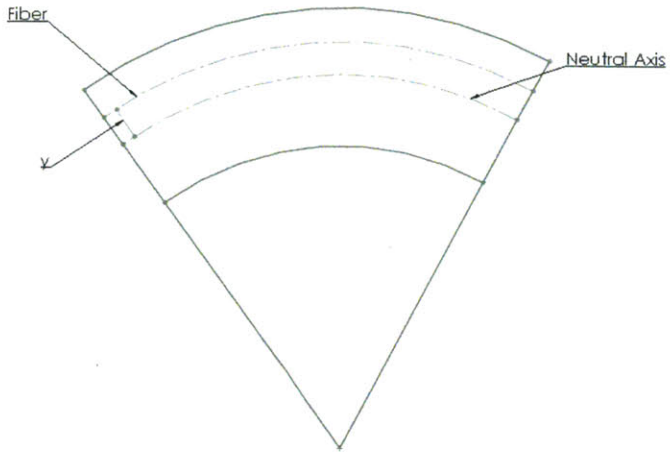

Figure for sheet bending showing measure y

The strain in the final rolled sheet is the summation of strain from heat induced curvature and the curvature induced to bring the sheet to its final shape:

$$\epsilon_f = \epsilon_b + \epsilon_h \rightarrow \epsilon_b = \epsilon_f - \epsilon_h \qquad (1)$$

From classical mechanics the strain in the final state is:

$$\epsilon_f = \frac{y}{\rho_f} \ (2)$$

The strain induced by the thermal gradient is:

$$\epsilon_h = \alpha \Delta T \left(\frac{y + \frac{t_0}{2}}{t_0} \right) \quad (3)$$

$\frac{t_0}{2}$ is included because $y = y_h - \frac{t_0}{2}$, y_h is measured from the bottom of the sheet.

Actual final stress: $\sigma = E\epsilon_b$ (4)

Inserting expressions for ϵ_f from (2) and ϵ_h from (3) into (1) then all into (4):

$$\sigma = E \left\{ \frac{y}{\rho_f} - \alpha \Delta T \left(\frac{y + \frac{t_0}{2}}{t_0} \right) \right\} \quad (5)$$

The stress in the sheet had it ben bent to final shape with no heat is :

$$\sigma_b = E\frac{y}{\rho} \quad (6)$$

Finally the relieved stress is: $\sigma_b - \sigma$

$$\sigma_r = E\alpha\Delta T\left(\frac{y+\frac{t_0}{2}}{t_0}\right) \quad (7)$$

At the outer fiber where: $y = \frac{t_0}{2}$

$$\sigma_r = E\alpha\Delta T \quad (8)$$

In the case of the G10 sheet:

E	2700Kpsi
α	6.6e-6ppm/°F
ΔT	400°F

Table 10

Inserting these values into (8) gives 7.1Kpsi relieved, which is significant enough to warrant the implementation of a simple heatsink to avoid thermal fatigue in the G10 sheet during soldering. The stress relief is greater as ΔT increases, so a more effective heat sink improves stress relief. Soldering is carried out at 660°F and and this analysis assumes a heatsink can provide an inner surface temperature of 260°F for a ΔT of 400F.

5. Brain Degasing

5.1. The Problem

The brains used for ex-vivo scanning are fixed in a preservative PLP solution. During the removal and fixation process air is introduced into the brain. There is no control over the initial processes that introduce the air because the removal and fixation processes are done elsewhere and arrive with air already introduced. Bubbles tend to get trapped deep in the sulci. Figure 70 shows an image in the sagittal plane from an ex-vivo scan, the artifacts caused by the bubbles are the black spots. Trapped air bubbles are a significant problem because they distort and obscure the high resolution scans, sometimes to the extent that the image is useless.

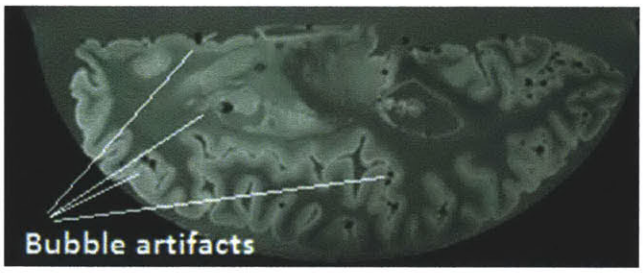

Figure 70

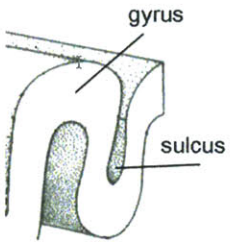

Figure 71

5.2. Removing bubbles

The main method utilized in this work to remove bubbles is vacuum. The concept behind this is to allow the bubbles to expand under the decreased pressure and push themselves out of their pockets and/or be removed by buoyant forces. The holders are incorporated into this vacuum process and serve as the vessel in which the brains are vacuumed and filled with PLP. Figure 72 shows the setup for the vacuum degassing. The basic procedure was: 1) pull vacuum on holder with the brain inside 2) open the PLP fill valve to fill the holder with fixative until full then seal off the fill valve 3) Begin the vibration and continue vacuum application for a predetermined time period (usually 2-6 hours). This filling method proved to be a very tidy way to pump PLP into the holder and minimizing user exposure to the solution. All this is carried out in a fume hood because of the vapor produced by the PLP solution under vacuum.

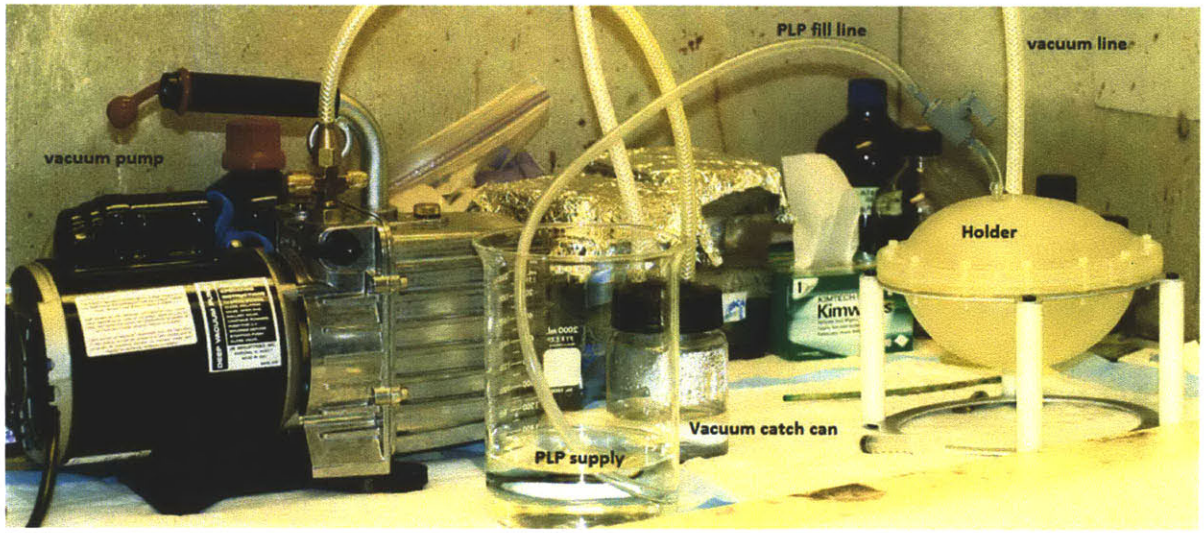

Figure 72

5.3. Vacuum only Test

The first degasing method tested used vacuum only. Figure 73 is from an MRI scan of one of the ex-vivo brains degassed and packed using a previous method. Note the high number of artifacts from the bubbles (black blooms and spots in the brain) especially deep in the sulci. Compare this to the results of the vacuum only method shown in Figure 74 which has almost no deep bubbles, only surface bubbles. The success of the vacuum only method warranted the exploration of additional methods to improve the process.

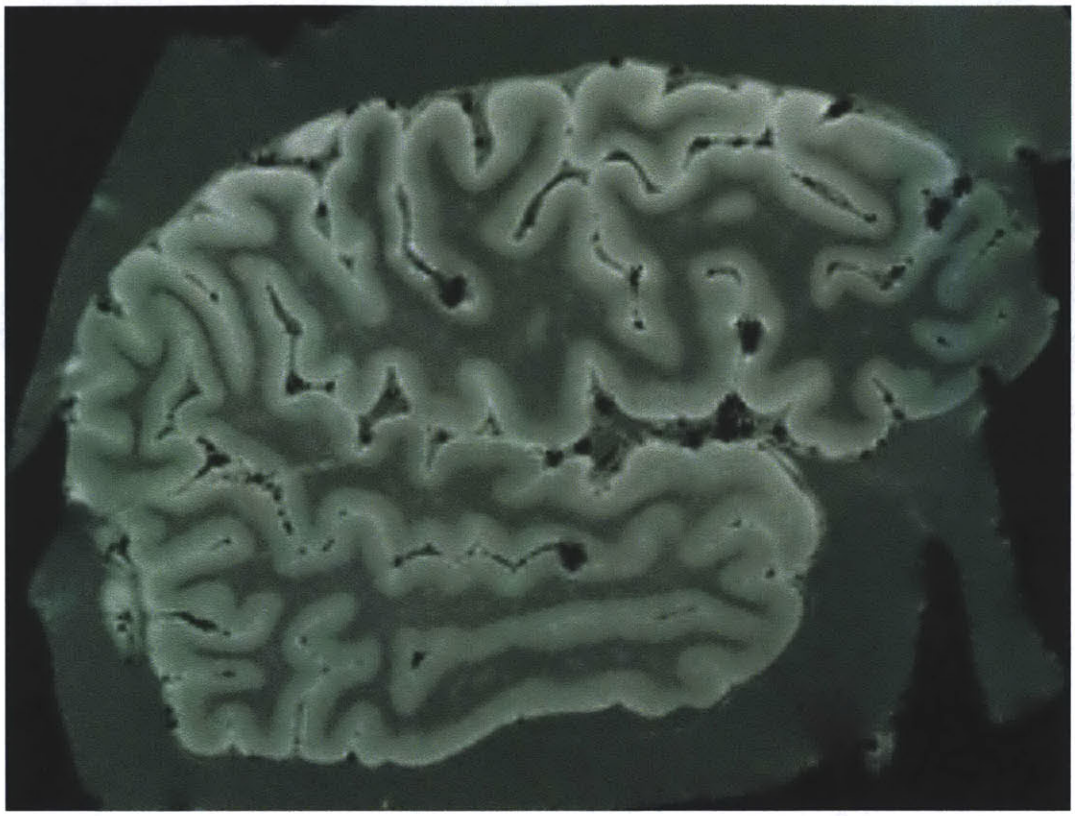

Figure 73

Results of traditional packing method

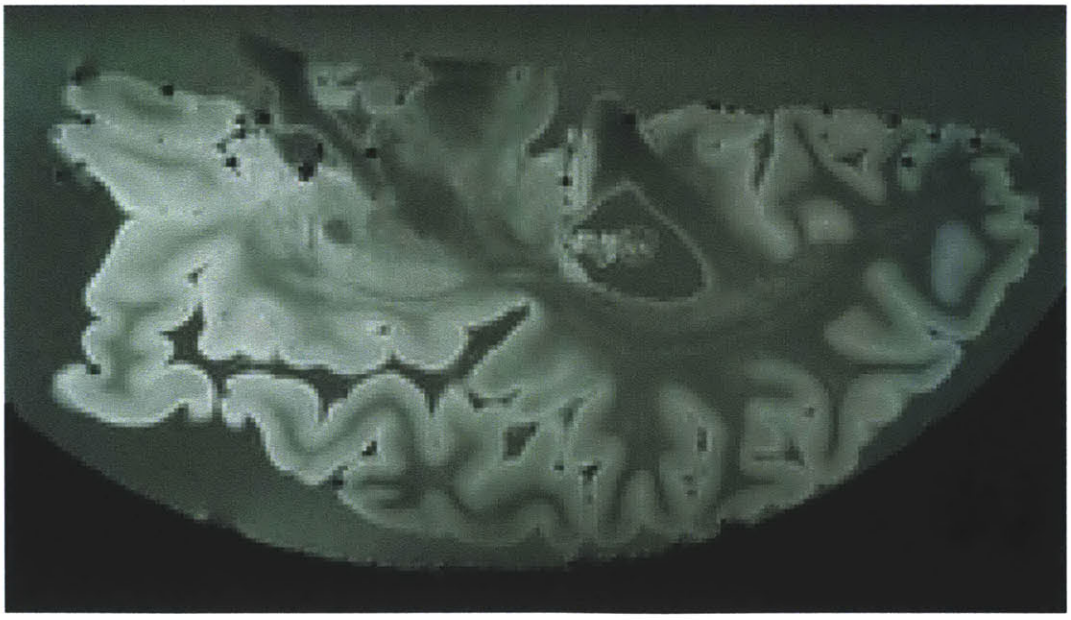

Figure 74

Results from using new holder and vacuum only

5.4. Vibration Under Vacuum

5.4.1. Shake, Rattle, and Roll apparatus

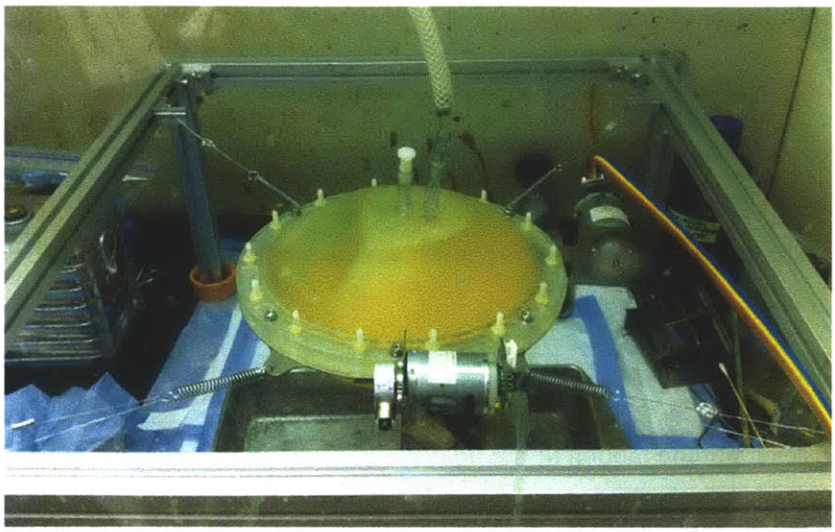

Figure 75

Shake apparatus

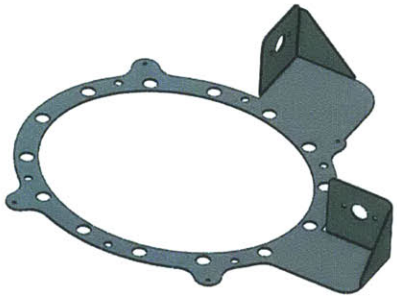

Figure 77

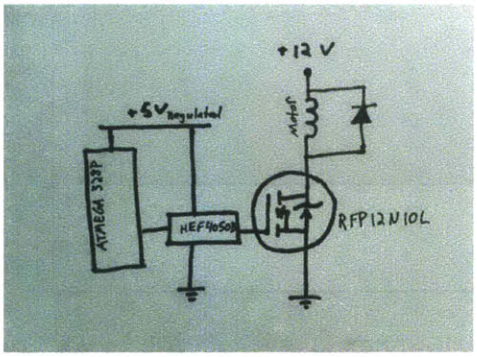

Figure 76

During an initial degasing test it was found that tapping the holder was incredibly effective at removing the remaining bubbles while under vacuum. This led to the concept of vibrating the holder to help remove bubbles. Vibration is used as an air removal method in applications like concrete pouring and inkjet printing (14). A prototype shaker mechanism (Figure 77) was constructed from folded and welded 1018 steel sheet that was cut on an OMAX waterjet. Two motors were mounted 90 degrees from each other with eccentric masses on the output shafts. The amount of eccentricity was adjustable by adding washers to a cap head screw on the heavy side of the eccentric. Average force inputs were around 4N at a max of 2000rpm. A pulse width modulation controller was made with an ATMEGA328p microcontroller, MOSFET, buffer, and diode to control the frequency of vibration.

The vibration chassis was suspended by soft springs in a frame such that all 6 rigid body modes were 2Hz and under. The unit was tested with a hemisphere brain sample which was known to contain stubbornly trapped bubbles from previous MRI scans. The sample was subject to vacuum and vibration in the degasing apparatus while completely submerged in PLP solution.

5.4.2. Initial shake test results

Large quantities of bubbles were observed leaving the brain for up to two hours after initiating the vibration. This is after vibration alone and vacuum alone ceased to remove any air. Table 5 summarizes some of the initial results. The test was stopped after two hours for MRI scanning to confirm that the air removal had been effective.

Frequency	Effect
2Hz	Large amplitude motion of the holder around the brain, some bubble removal
10-20Hz	Violent agitation of bubbles, massive bubble removal, vibration chassis bending modes excited

Table 11

A 500 micrometer MRI scan revealed a marked decrease in bubbles over all previous tests, however the bubbles were not completely eliminated and some bubbles remained on the top surface of the brain. These initial results were promising enough to warrant the construction of a devise to provide shaking and automatic vacuum control so that degassing sessions could run for hours unattended.

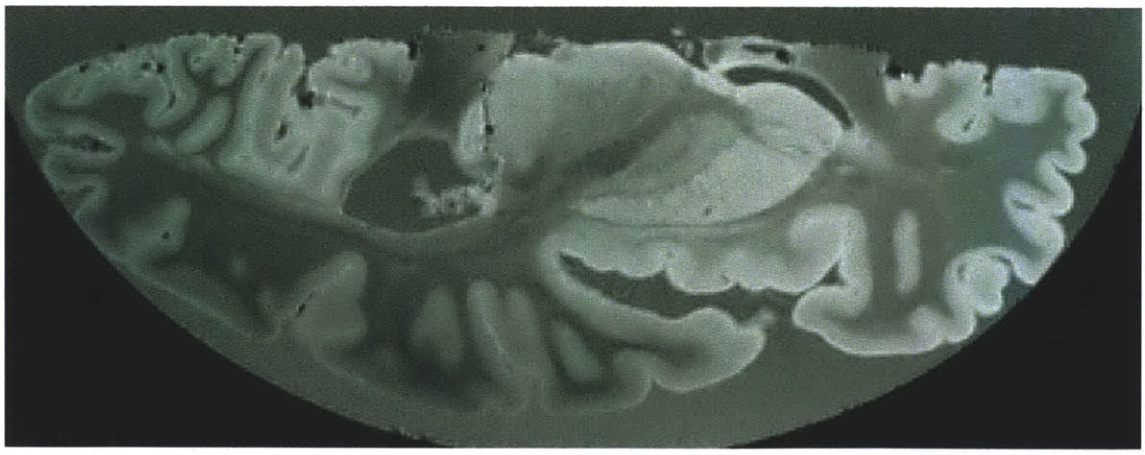

Figure 78

Results from shake test 1, vacuum and vibration applied

5.4.3. Shake Test : Surfactant and Frequency Sweep

Figure 79 shows the results of a second bubble removal test which employed a surfactant in the PLP solution to lower surface tension, and a vibration sweep from 0-20Hz-0 over a 20 second period. The test was run for 4 hours continuously and the brain scanned after 1 week of storage due to MRI availability restrictions. Note the nearly complete removal of bubbles from the bulk of the brain. The only remaining bubbles are on the upward facing surface of the brain which can be removed by flipping the brain halfway through the degas process. Compare this to Figure 73 which shows the original packing method; note the decrease in the artifacts (black spots) caused by the bubbles.

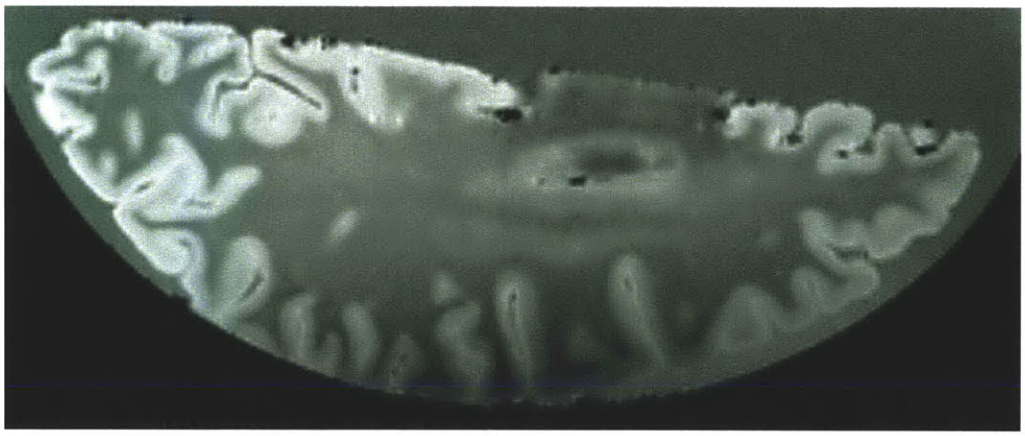

Figure 79

Shake test 2 results, vacuum, vibration, and surfactant applied

6. Conclusions

Ex vivo coil assemblies are "one-off" designs, each design fulfills a different need or is an iteration of previous work. They are built in lab; the exploratory nature of the process and the need to iterate demands flexible, low cost, and rapid manufacturing methods. In this project a unique set of existing and newly developed tools and design methodologies are brought together in the development and construction of a 32 channel 7T ex vivo coil. These manufacturing tools and design methods are intended to provide the flexibility and capability to produce components with increased accuracy and improved properties while expanding the limits of what is possible to build in-lab. Increasing coil building ability opens the possibility of developing a wide range of custom coils to improve both *in* and *ex* vivo MRI imaging. This results in faster iteration on coil designs and improved imaging. The hope is that improved coil designs will help speed research of brain disorders and also improve in vivo imaging for early detection and treatment of disease and injury. The tools and methodologies in this work need not be restricted to MRI coil design. They can and should be applied and adapted to any prototyping work that requires low-cost, time efficient methods and tools.

7. Future Work and Design Improvements

7.1. Quantify Receiving Array alignment sensitivity

Sensitivity to positioning the receiving former halves relative to each other will be quantified. After the 32 channel 7T assembly is complete bench tests will be done to determine the effect of 1-5mm misalignments in the X, Y, and Z directions. If deemed necessary a kinematic mounting could be used to ensure repeatable positioning of the receiving formers relative to each other. Figure 80 shows a concept for a possible quasi-kinematic mount. Three pins are used to locate the top former with each pin held between a set of flexures.

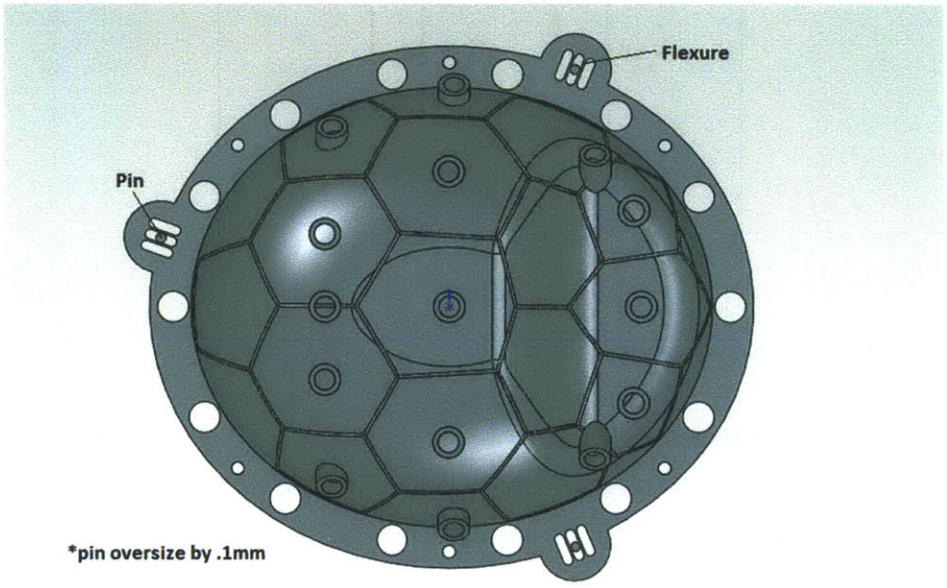

Figure 80
Flexural kinematic mount (24)

7.2. MRI Vibration Environment

The vibration spectrum at the MRI bed needs to be measured for the variety of scan sequences. A dynamic model can be created for the birdcage/ receiving array and this data can be used as an input. With this, designs can be optimized for minimal dynamic response. This data could also be used to design a vibration isolation base that simply bolts onto the current design and replace the base.

There are some significant challenges in gathering vibration data due to the extreme magnetic fields. Direct measurement with accelerometers is a challenge because magnetic materials are not allowed near the MRI and the high field strengths induce current in instruments and cables. Another option would be

laser or optical vibrometry which can measure vibration at a distance. However the camera or laser would need to be placed sufficiently far away from the MRI, probably outside of the MRI cell.

7.3. Brain Holder Bolted Flange

In future designs bolts in the brain holder flange should be spaced such that 60° stress cones overlap. This can be accomplished by either thickening the flange, or decreasing the bolt spacing. This will reduce the chance of the holders leaking as the plastic relaxes over time. This design also reduces the bending stress in the flange by decreasing the distance between the zero-slope condition present at each bolt. **(15)**

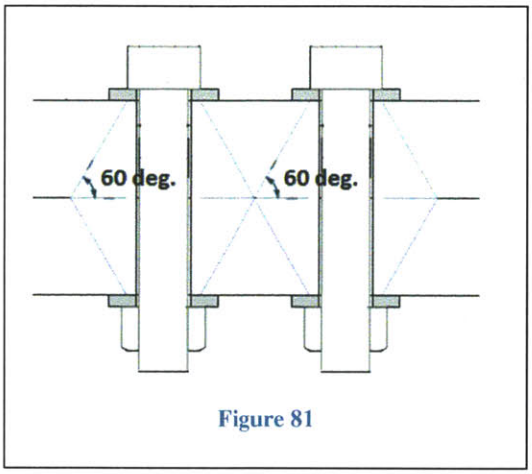

Figure 81

7.4. Continue Improving Degas Method

The degasing method will continue to be developed. I believe that the vibration and vacuum apparatus should continue being used and complete degassing can be achieved by increasing the degassing time.

Works Cited

1. *Detection of Entorhinal Layer II Using Tesla Magnetic Resonance Imaging.* **Jean Augustinack, et al.** 4, s.l. : Annals of Neurology, April 2005, Vol. 57.

2. *Predicting the Location of Entorhinal Cortex from MRI.* **Fischl .** 1, s.l. : Neuroimage, 2009, Vol. 47. ISSN 1053-8119.

3. Athinoula A. Martinos Center for Biomedical Imaging. [Online] http://www.nmr.mgh.harvard.edu/martinos/flashHome.php.

4. *Size-optimized 32-channel brain arrays for 3 T pediatric imaging.* **Keil, B., Alagappan, V., Mareyam, A., McNab, J. A., Fujimoto, K., Tountcheva, V., Triantafyllou, C., Dilks, D. D., Kanwisher, N., Lin, W., Grant, P. E. and Wald, L. L.** 6, s.l. : Magnetic Resonance in Medicine, Vol. 66. doi: 10.1002/mrm.22961.

5. *Unsolved Problems in Comparing Brain Sizes in Homo Sapiens.* **M. Peters, L. Jäncke,J.F. Staiger,G. Schlaug,Y. Huang,H. Steinmetz.** 2, s.l. : Brain and Cognition, 1998, Vol. 37.

6. *An Efficient, Highly Homogeneous Radiofrequency Coil for Whole-Body NMR Imaging at 1.5 T.* **C. Hayes, W. Edelstein, J. Schenck, O. Mueller, M. Eash.** s.l. : Journal of Magnetic Resonance, 1985, Vol. 63.

7. *The NMR Phased Array.* **P.B. Roemer, W.A. Edelstein, C.E. Hayes, S.P. Souza, O.M. Mueller.** s.l. : Magnetic Resonance in Medicine, 1990, Vol. 16.

8. **D. Weyers, S. Le, D. Dean.** *RF Birdcage coil with reduced acoustic noise. 6,661,229* Dec 9, 2003.

9. **John Uicker, Gordon Pennock, Joseph Shigley.** *Theory of Machines and Mechanisms.* New York : Oxford Press, 2003.

10. *Durometer hardness and the stress-strain behavior of elastomeric materials, Rubber Chemistry and Technology.* **Qi, HJ and Joyce, K. and Boyce, MC, pp. 419-435.** 2, 2003, Vol. 76.

11. **Kalpakjian, S. Schmid, S.** *Manufacturing Engineering and Technology 5th ed.* 2006.

12. Matweb results for extruded polycarbonate. *Matweb.com.* [Online] Matweb Materials Database. http://www.matweb.com/search/DataSheet.aspx?MatGUID=501acbb63cbc4f748faa7490884cdbca&ckck=1.

13. The Center for Functional Neuroimaging Technologies. [Online] http://www.nmr.mgh.harvard.edu/martinos/ncrr/index.

14. **Lim, Su-min.** *Apparatus to remove bubbles in an inkjet printer. 7585064* Sept. 8, 2009.

15. **Slocum, Alexander H.** *FUNdaMENTALs.* Cambridge : Massachusetts Institute of Technology, 2008. pp. 9-9.

16. **Bharath, A.A.** *Introductory Medical Imaging.* s.l. : Morgan and Claypool, 2009.

17. Freeman Supply, Fast Cast data. [Online] http://www.freemansupply.com/tables/renfastcast.htm.

18. **Company, Hexion Chemicals.** Epon 3234 technical datasheet. [Online] http://www.hexion.com/Products/TechnicalDataSheet.aspx?id=3994.

19. **Supply, Freeman.** Repro NS material data. [Online] http://www.freemansupply.com/datasheets/Freeman/Repro/ReproNS.pdf.

20. **Corp., Renishaw.** Renshaw Vacuum Casting. [Online] http://www.renishaw.com/en/5-01-ulc-vacuum-casting-machine--15269.

21. **Database, Matweb Material.** G-10 Fiberglass Epoxy Laminate Sheet . [Online] http://www.matweb.com/search/DataSheet.aspx?MatGUID=8337b2d050d44da1b8a9a5e61b0d5f85.

22. *MR Physics.* **Makhoul, Khaldoun.** Boston : Massachussets General Hospital, 2011.

23. **Hibbeler, R.C.** *Mechanics of Materials 7th ed.* Upper Saddle River New Jersey : Pearson Prentice Hall, 2008.

24. **Scherz, Paul.** *Practical Electronics for Inventors.* s.l. : McGraw Hill, 2007.

25. *MTL Grant renewal.* **Fischl, Bruce.** Boston, MA : Martinos Center for Biomedical Imaging, 2012.

26. **Slocum, Alexander H.** *Flexural kinematic Mount Concept.* Cambridge MA, 2012.

Appendix A

Creating Preamp Layout Features on an Ex Vivo Receiving Coil Former

*This guide assumes a certain level of proficiency with SolidWorks. It requires creating part features in the context of an assembly, using more advanced sketch entities, tricky swept cuts, and the ability to control feature relations.

1) Using a 3d sketch, layout points on the surface of the former that are approximately at the center of each coil center. Create only one side, mirror points across medial plane.

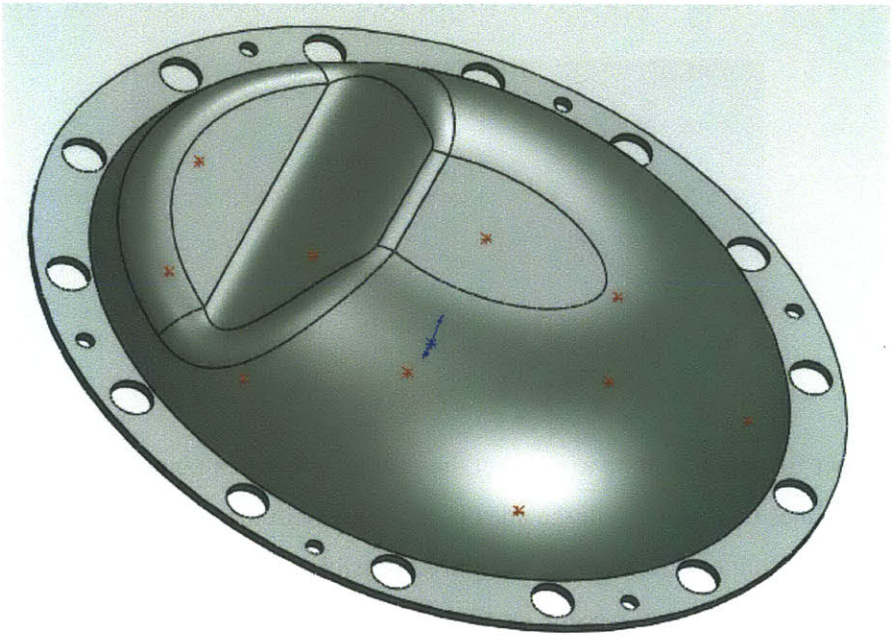

2) Create planes using the former surface and a point from step 1. as references, there should be one plane for every point.

3) Create two new parts, one a planar hexagon, one a pentagon. Estimate sizes for now, they will need adjusting as you iterate. In an assembly mate these hexagons and pentagons with the former by making the center point of the hexs. and pents. coincident with the points created in step 1. Adjust the size and orientation of the hexs. and pents. as well as locations by moving the layout points. Iterate until the shapes cover as much area and fit as tight together as possible.

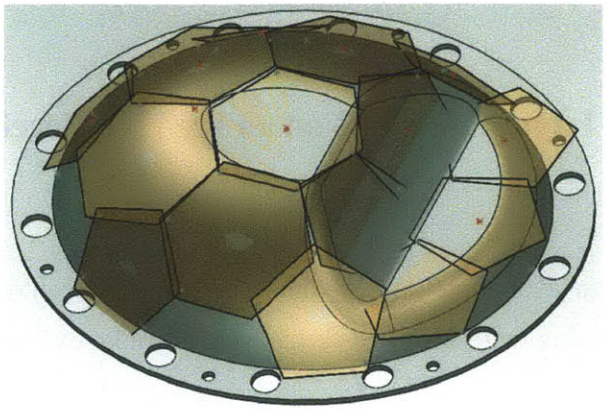

4) Inside of the assembly, while editing the former part, place points (again using 3d sketch) at the apexes of the hexs and pents. Where apexes overlap, try to place a shared point at the center of all the apexes. See the green dots below. These dots will all be connected to create your "soccer ball" mesh.

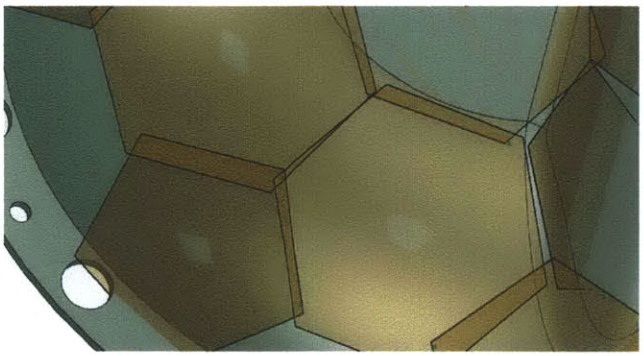

5) Back in the former file it's now time to connect the pent and hex apex points. To do this use "spline on surface" to create lines that connect all the apex points laid out in the assembly (use only two points, start and finish, for each spline so lines are as straight as possible). Check carefully to be sure the splines actually lay on the surface, instead of passing through the surface. The figure below shows an example. The shapes will inevitably require some tweaking to maximize coverage and create as uniform shapes as possible.

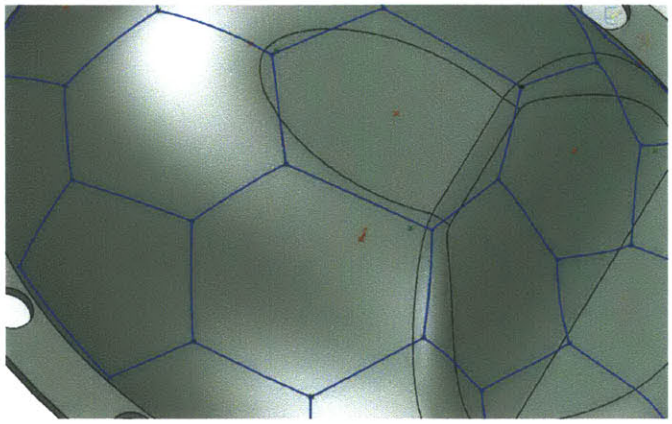

6) These lines will now be used as guide paths for a swept cut feature. The swept cut cannot be self-intersecting so to cut all the features will require several swept cuts. Inside the swept cut manager, right click in path entry box and use "edit selection" or "selection manager" then click the select group icon

and start selecting sections of the sweep cut path. Select an open, non-intersecting set of segments. If SolidWorks will not solve try selecting only one or two segments of the path at a time, create the feature. If SolidWorks solves, go back and add one or two more segments. Do this as long as you can to avoid having to create many new cut cross-section reference planes and profile sketches.

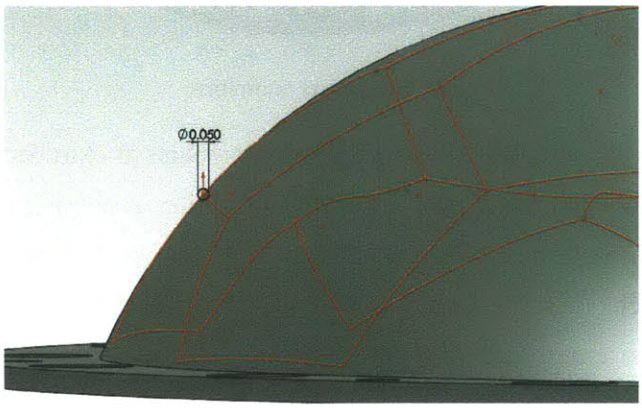

Swept cut cross section sketch

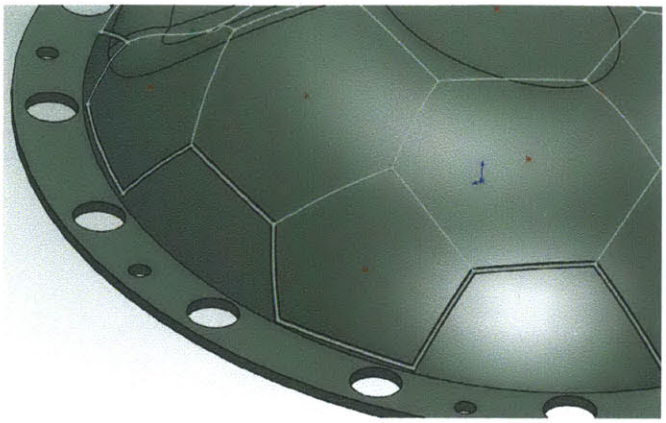

One swept cut

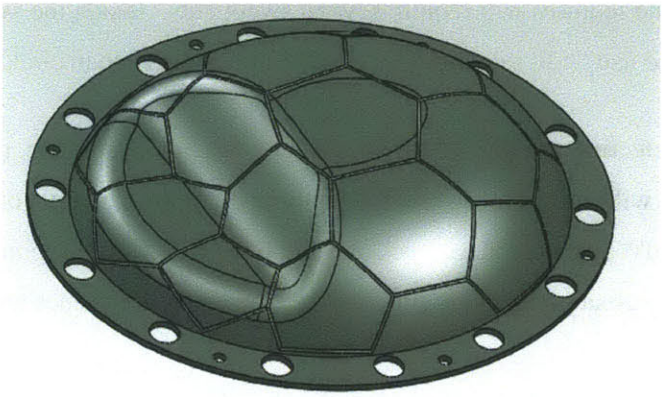

All swept cuts complete

7) The coil layout features are complete, now add in preamp mounts as extruded features. The "extrude up to next" option is helpful here. Place as many extrusion profiles as possible on the same plane. Some tilted mounts will require their own sketch plane. Adjust and tweak the mounts to avoid placing preamp inputs and outputs near each other. Inputs and outputs must be at least one pre-amp length away from each other. Trim mounts to appropriate heights with extruded cut.

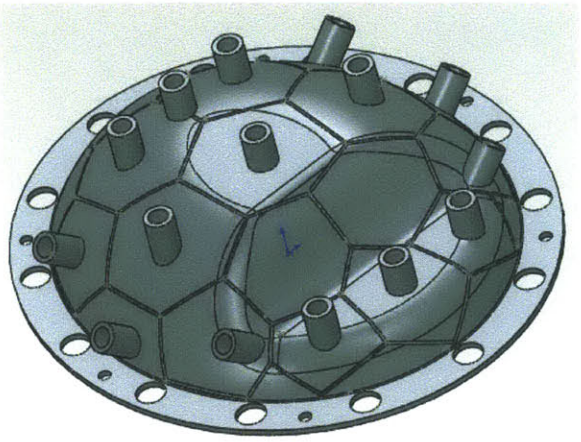

Former with pre-amp mounts.

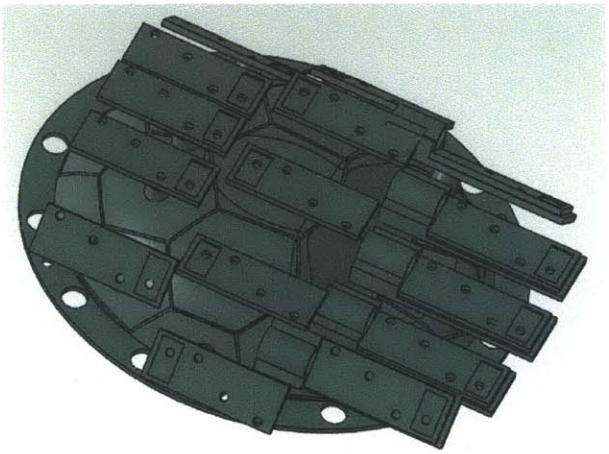

Former with pre-amps mounted. Square indentation is the input end. Note how no inputs are near other outputs. Boards on right hand side have cable traps installed.

Appendix B

Using the Desktop Vacuum Casting Setup

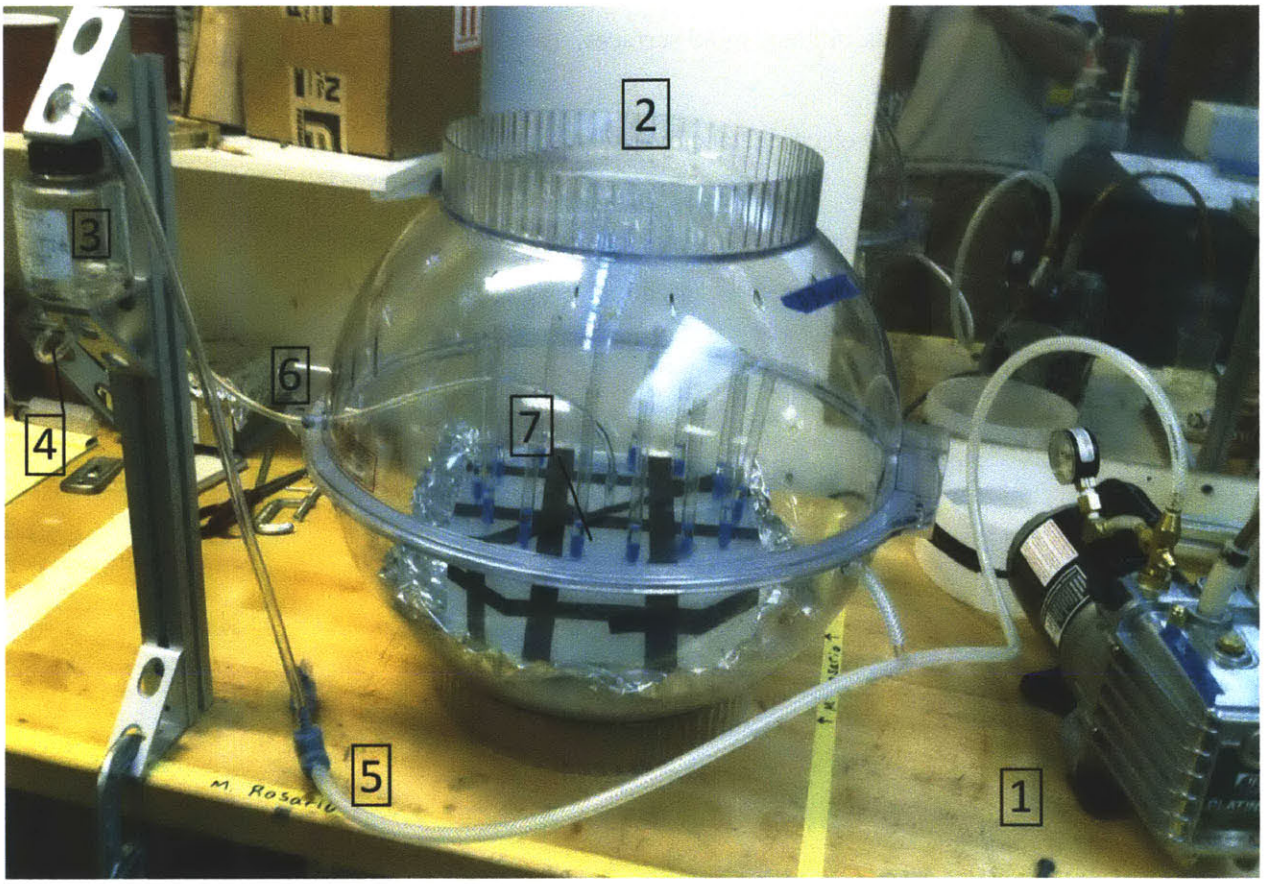

1	Vacuum pump
2	Vacuum Chamber (Secador® Techni-Dome® 360 Vacuum Desiccator)
3	Resin supply
4	Resin line pinch off
5	Vacuum control line (allows degassing of resin in tandem with mold pump-down)
6	Resin line feed-thru

The pictured setup is a very simple configuration that keeps the resin supply pot external to the chamber. This allows resin to be added during the casting process if needed. The vacuum line running to the resin supply pot allows the resin to be degassed in place and is advantageous because filling can begin as soon as the resin is degassed. The other option is to degas the resin inside the vacuum chamber in a separate

process. This takes extra time and may not be possible for resins with short gel-times. The foil is to keep spilled resin off the chamber.

Steps:

1. Apply release agent to the silicone mold surfaces. Freeman's Pattern Release 202 was used for this work.
2. Close the mold and apply electrical tape over seam and around mold body to help keep mold together during fill.
3. Insert risers: 1/2 " rigid plastic tubing was used here. The risers need to hold enough material to supply collapsing voids during re-pressurization.

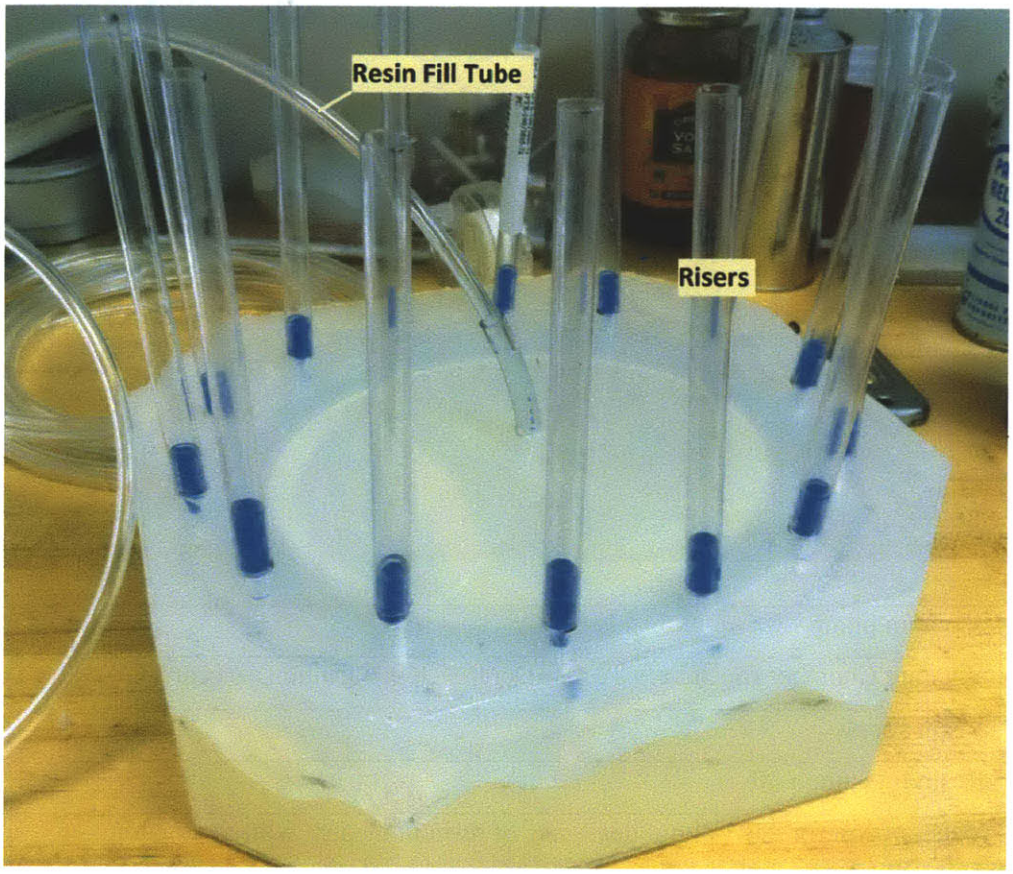

4. Insert resin supply line which runs from the mold through the vacuum chamber wall, through a flow control mechanism and into the bottom of the resin supply pot

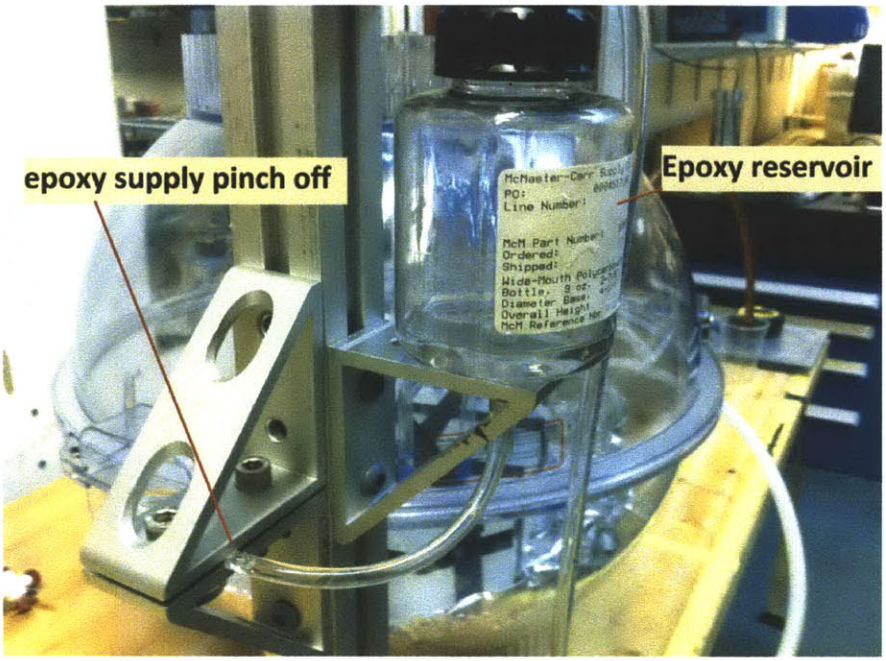

5. Insert mold into vacuum chamber and seal chamber, close off flow control. The flow control here is very basic but effective; the two bolts pull the plates together and restrict the tube. Control is provided by tightening or loosening the bolts.
6. Pump down the vacuum chamber to casting pressure. If pressure is too low, epoxy may foam due to evaporating volatiles. No amount of epoxy degassing will cure this.
7. When desired pressure is reached in chamber, slowly open resin flow control until a slow steady flow is achieved. Watch for mold ballooning, bulging, or seam separation, these symptoms indicate exceedingly fast fill rates.

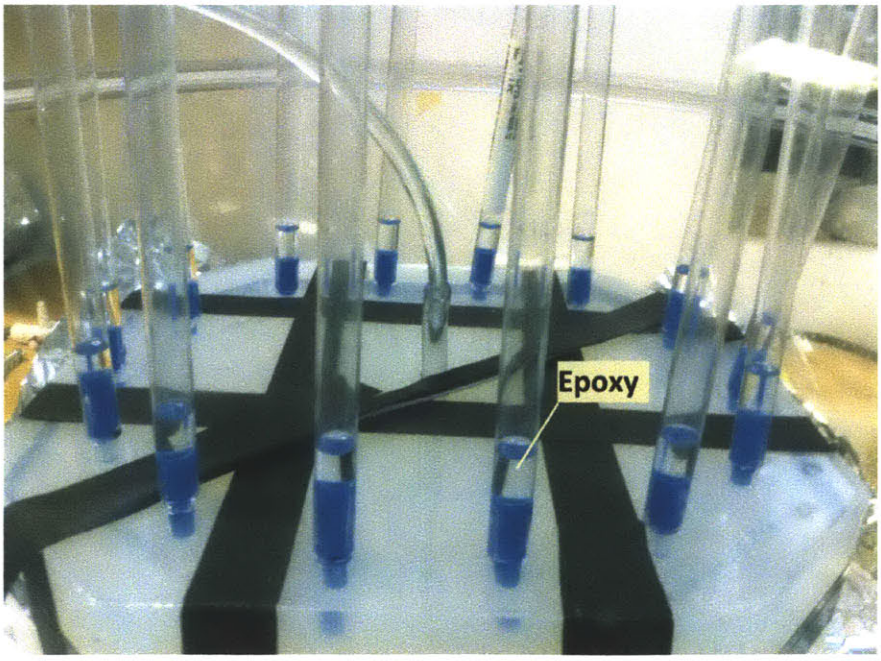

8. Continue filling monitoring resin supply. Stop filling when resin supply is nearly empty.
9. Re-pressurize the vacuum chamber to atmospheric pressure. Any collapsing voids will draw excess resin in from the resin supply line or risers.
10. Allow part to cure